NASA TECHNICAL NOTE

NASA TN D-4178

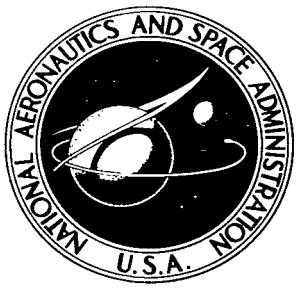

EXPERIMENTAL HEAT-TRANSFER STUDY OF A REGENERATIVELY COOLED HYDROGEN-FLUORINE ROCKET ENGINE AT LOW CHAMBER PRESSURE

by Arthur N. Curren, Harold G. Price, Jr.,
Roger C. Krueger, and Frank L. C. Manning

Lewis Research Center
Cleveland, Ohio

NATIONAL AERONAUTICS AND SPACE ADMINISTRATION • WASHINGTON, D. C. • SEPTEMBER 1967

NASA TN D-4178

EXPERIMENTAL HEAT-TRANSFER STUDY OF A REGENERATIVELY COOLED HYDROGEN-FLUORINE ROCKET ENGINE AT LOW CHAMBER PRESSURE

By Arthur N. Curren, Harold G. Price, Jr., Roger C. Krueger, and Frank L. C. Manning

Lewis Research Center
Cleveland, Ohio

NATIONAL AERONAUTICS AND SPACE ADMINISTRATION

For sale by the Clearinghouse for Federal Scientific and Technical Information
Springfield, Virginia 22151 – CFSTI price $3.00

EXPERIMENTAL HEAT-TRANSFER STUDY OF A REGENERATIVELY COOLED HYDROGEN-FLUORINE ROCKET ENGINE AT LOW CHAMBER PRESSURE

by Arthur N. Curren, Harold G. Price, Jr., Roger C. Krueger, and Frank L. C. Manning

Lewis Research Center

SUMMARY

An experimental investigation was conducted to determine heat-transfer rates and coefficients as well as coolant pressure-loss characteristics in regeneratively cooled liquid hydrogen-liquid fluorine rocket engine thrust chambers. The chambers were operated at a combustion pressure of about 60 pounds per square inch absolute and propellant mixtures of about 12, 15, and 18 percent hydrogen by weight, yielding a nominal thrust level of 1000 pounds at sea-level conditions. The nozzle throat design diameter was 3.910 inches, and design contraction and expansion ratios were 1.897 and 3.679, respectively. The chambers were of cylindrical, right-conical construction, and the cooling system was such that the incoming fuel (hydrogen) was ducted in a jacket along the nozzle and combustion zone external surfaces from nozzle exit to injector in a single pass. Injectors used were of multielement coaxial design and had been developed to yield smooth, high-performance operation with the thrust chambers used in this investigation. Instrumentation consisted of specially constructed small-diameter thermocouple assemblies embedded in the thrust-chamber walls, others inserted into the coolant stream, and conventional static-pressure taps in the coolant channels, all at several different positions along the length of the thrust chamber.

Local combustion gas-to-wall and wall-to-coolant heat-transfer rates and coefficients as well as coolant pressure-loss characteristics were determined by data analysis. This information made possible the derivation of appropriate constants for modifications of a dimensionless heat-transfer correlation for local application. In addition, the coolant friction pressure-loss factors were compared with the values predicted by means of a familiar smooth-tube correlation. Pertinent data and the consequent results are included in graphic and tabular form in this report.

INTRODUCTION

For lightweight, high-energy rocket engines to be used for long firing durations or rapid-sequence short-term intermittent operation, a thrust-chamber cooling system is required because of the high temperature and heat flux levels involved. Perhaps the simplest cooling scheme is a single-pass regenerative system, in which one of the propellants is used to convectively cool the nozzle and combustion zone portions of the thrust chamber. In order to design such a cooling system so that a safe wall temperature level, and consequently structural integrity, is assured, a method is required for the accurate prediction of local wall and coolant temperatures and heat-transfer rates between combustion gas and walls and also between walls and coolant. Further, in order to effectively prescribe flow system components, it is essential to have good knowledge of the coolant's pressure-loss characteristics.

These required rates and characteristics are functions of the propellant combination, flow rates, combustion conditions, and thrust-chamber cooling system configuration. The interrelation of these variables, particularly for the prediction of gas-to-wall heat-transfer rates, is presently the subject of much confusion and controversy. A number of studies in this problem area, both analytical and experimental, have been performed by NASA and others. These studies have yielded proposed correlations for gas-to-wall and wall-to-coolant heat transfer, but general agreement has not yet been achieved. It is the purpose of this investigation to contribute further carefully obtained experimental information to this problem area with a view to the eventual reaching of a general solution.

Appropriately instrumented rocket thrust chambers using the propellant combination liquid hydrogen and liquid fluorine, a combination selected because of its desirable combustion and performance characteristics, were operated to obtain the data for this study. The propellant mixtures investigated were nominally 12, 15, and 18 percent fuel by weight, giving rise to a thrust level of about 1000 pounds with a combustion pressure near 60 pounds per square inch absolute. To assure reasonably long hardware life, these propellant mixtures were chosen well away from the stoichiometric, higher temperature mixture of 5.038 percent fuel by weight. The combustion pressure, 60 pounds per square inch absolute, was selected in part because of the anticipated interest in a simple, reliable, low-chamber-pressure, pressure-fed, high-performance propulsion system for upper-stage space-vehicle application. The physical dimensions of the thrust chambers were selected primarily for convenience in this heat-transfer study and are not intended to imply a recommended configuration for any other application. Injectors were employed which had been developed, in a separate phase of this study, to yield stable, high-performance combustion conditions with the thrust chambers studied here.

APPARATUS

Thrust Chambers

The two thrust chambers utilized for this study were, except for instrumentation, of identical cylindrical, right-conical design. Configuration details are shown in figure 1. The nozzle throat design diameter was 3.910 inches, and design contraction and expansion ratios were 1.897 and 3.679, respectively. The distance from the injector edge line to the throat was 11.91 inches, and the nozzle's divergence half-angle was 15 degrees. This thrust-chamber configuration gave rise to a sea-level thrust of about 1000 pounds for the operating conditions considered in this study. This chamber design is essentially the same as that developed in reference 1.

These thrust chambers were of "channel-type" construction, wherein a number of preformed channel members are positioned so that their bottom segments form the thrust-chamber internal wall, as shown in figure 1. The number of channels (72 here) is determined primarily by strength of materials considerations. The radial channel webs separate the inner and outer chamber walls, forming the coolant flow path. The channel material used in this study was 0.022-inch-thick type 304 stainless steel, and the braze-attached outer wall was a wrap of rectangular section 0.040-inch-thick type AM 350 stainless-steel wire. A more detailed description of the fabrication process appears in appendix A.

An annular manifold was located at the nozzle exit end of the thrust chamber to receive the incoming liquid hydrogen coolant as shown in figure 1. From this manifold, the hydrogen was directed by means of a distribution plate to the 72 coolant channels, in which it flowed the length of the chamber. At the injector end of the chamber, the hydrogen entered another manifold, from which it was ducted into the injector and subsequently into the combustion chamber. The fluorine, not being used as a coolant, passed directly into the combustion chamber through the injector.

The specification of coolant channel heights (the only variable dimension, since the number of channels and consequently channel width is fixed at every axial position), was based on a design method indicated in reference 2. The combustion gas thermodynamic and transport properties used in the original design were later found to be in error and have since been reevaluated. A comparison of the original design and experimental values such as wall temperatures or heat fluxes are not included in this study. The thrust chambers operated successfully in the ranges of this study, although of course the original design values were not realized.

The pertinent coolant channel dimensions for the thrust chambers used in this study, to be referred to as chambers 1 and 2, are listed in table I, along with their corresponding axial positions. The average channel heights are tabulated, along with the specific

heights and cross-sectional flow areas for the two instrumented channels. The use of these dimensions will be indicated in the section CALCULATIONS AND RESULTS in this report.

Propellants

The propellant combination used here, hydrogen and fluorine (H_2-F_2), was selected for several reasons, each of which is important with respect to this study. First, it has a high combustion temperature, giving rise to relatively high heat flux levels for these conditions. Second, since the thrust chambers were heavily instrumented with rather fragile sensors, the characteristic smooth, spontaneous ignition of hydrogen and fluorine even at low pressures is obviously advantageous. Further, destructive combustion instabilities have never been observed, to the knowledge of the authors, over the wide range of operating conditions which have been studied at the Lewis Research Center and elsewhere. High performance (characteristic velocity efficiency) and stability have been demonstrated over a wide range of fuel weight fractions with a fixed injector, indicating a clear advantage over some other propellant combinations from the standpoint of efficient hardware utilization. Also of importance is the fact that experimental performance data obtained with thrust chambers of the type used in this study (ref. 1) and with even larger expansion ratios (refs. 3 and 4) indicate nearly ideal equilibrium composition of the combustion gases, making this assumption in data analysis a reliable one. Three propellant mixtures (12, 15, and 18 percent hydrogen by weight) were selected to determine possible mixture effects on the thrust-chamber heat-transfer characteristics.

From an operations point of view, the handling of the propellants used here is not a difficult or particularly hazardous procedure. Over a period of several years, a large amount of liquid and gaseous fluorine has been used at the Lewis Research Center. As a result, a great deal of experience has been gained relative to the selection of compatible materials, fabrication, cleaning, and operations. Consequently, quite reliable fluorine handling and operating procedures have evolved. Relatively standard procedures govern the use of hydrogen.

Combustion-gas properties. - The equilibrium composition and other thermodynamic properties of the products of combustion of hydrogen and fluorine were calculated by means of the programs of references 5 and 6. The transport properties were computed by means of the method described in reference 7. Since properties for this propellant combination computed by these means have not been published, a very brief summary of the values used in this study is presented in table II. In table II, specific heat, viscosity, thermal conductivity, and enthalpy are tabulated at some temperatures for the three fuel weight fractions considered here (12, 15, and 18 percent hydrogen by weight) for three

pressures, 60, 37.3, and 14.7 pounds per square inch absolute. Also tabulated are static temperature and pressure values as functions of chamber area ratio, computed on the basis of a reversible adiabatic flow process assumption. While the thrust chambers used in this study were cooled, the heat removed was estimated to be very small compared to the total energy released by the propellants. The use of the tabulated static temperature and pressure schedules was therefore assumed to be justified. In addition, table II includes information for the off-pressure correction of the characteristic velocity performance parameter.

Coolant properties. - An evaluation of the storage time and conditions for the liquid hydrogen used in this study indicates the hydrogen would be essentially entirely in para form at the time of its use. Consequently, the properties of hydrogen used here were for 100 percent para form and were calculated by the methods of reference 8.

Injectors

To satisfactorily determine the heat-transfer parameters investigated by this study, it was considered essential that the thrust chambers be operated without significant low-frequency combustion pressure oscillations and that local chamber wall "hot spots" be avoided. Since the injector plays a major role in these considerations, a preliminary effort in this study was the selection and development of suitable injector configurations to satisfy these requirements for the range of operating conditions to be considered. Two injector types were selected to be run with each chamber so that thrust-chamber heat-transfer characteristics dependency on injector configuration would be revealed, if it exists.

One of the injectors selected was the 121-element coaxial hexagonal-pattern unit shown in figure 2. This was a flight-weight configuration having a 0.084-inch-thick nickel face dished to a 20-inch radius of curvature. A detailed study of the performance of this injector type is presented in reference 9. The other injector style chosen was also of coaxial-element design, but having 131 elements in a ring pattern. This injector's face was 0.700-inch-thick copper and was flat, as shown in figure 2. Reference 4 describes the performance of this injector type.

Both of the injectors used, it should be noted, had continuous spray patterns, without any auxiliary fuel sprays around the perimeter for chamber film cooling. Also, both injectors had an element pattern density greater than 5 per square inch (5.31 for the 121-element injector and 5.75 for the 131-element one) which is indicated in reference 9 as required for high performance at essentially the pressure level considered in this investigation. The 121-element injector's spray pattern had a constant propellant flow rate per unit area over its entire face area, while the 131-element one had a constant unit

area flow rate for each ring in its pattern, but the rate varied a small amount from ring to ring.

In brief, the development study of the injectors indicated that chamber wall local "hot spots" did not occur, and that the fluorine pressure drop through the injector was the primary influence on low-frequency combustion pressure oscillations. When the orifice holes were sized so that the fluorine pressure drop exceeded about 29 pounds per square inch, oscillations were not significant. For the runs of this study, the oscillations indicated by means of a closely coupled helium-purged transducer never exceeded ±1.56-pound-per-square-inch amplitude with a frequency of about 560 cycles per second, considered here to be a satisfactory level. Actually, for most of the runs, oscillations were essentially nonexistent. The hydrogen injector pressure drop was kept between 10 and 20 pounds per square inch, a convenient level for the flow controller used.

Thrust-Chamber Instrumentation

Thrust chamber 1 had eight instrumentation planes along its longitudinal axis, as shown in figure 1. The stations were 1.5 inches apart, measured along the coolant flow path, with one station, F, at the nozzle throat. This station spacing was indicated by the size of the anticipated coolant temperature increase between stations. Each station had an instrument array as shown in figure 3(a). On the designated station plane two 0.020-inch-diameter thermocouple assemblies fabricated with 0.0025-inch-diameter Chromel-Alumel wires were embedded within the 0.022-inch-thick wall. One of these (thermocouple 4) was on the channel centerline, and the other (thermocouple 2) at a point one-fourth the channel inside width. Thermocouple details are indicated in figure 3, and a further description of instrument placement appears in appendix A. Located 0.12 inch upstream relative to coolant flow was a 0.020-inch-diameter thermocouple assembly fabricated with 0.0025-inch-diameter copper and constantan wires (thermocouple 3) inserted about 0.030 inch into the coolant stream on the channel centerline, and another identical instrument (thermocouple 7) located on the chamber wrap outside surface in line with the point of web-wrap attachment. Another Chromel-Alumel thermocouple (1) was located 0.24 inch upstream from the designated station plane at the junction of two adjacent channels on the hot-gas surface. At this same plane were located two copper-constantan thermocouples, one on the wrap outside surface on the channel centerline and another halfway up the channel web (thermocouples 5 and 6, respectively). Because of space restrictions, thermocouple 6 was used in stations G and H only. A 0.0625-inch outside diameter, 0.0125-inch wall thickness coolant static-pressure tap tube was located 0.19 inch downstream from the station plane. All the instrumentation described was placed in the same coolant channel at each station, called channel 1 in this study. With the exception of the pressure taps, these instrument arrays were duplicated in the

diametrically opposed coolant channel (to be called channel 2) to demonstrate symmetry. Physical space and data recording capacity limitations prevented additional coolant channel pressure measurements.

In addition to these instruments, the chamber's coolant inlet manifold was equipped with two carbon resistor thermometers inserted into the coolant stream and a pressure tap. The injector-end coolant manifold had four copper constantan thermocouples (not alined with the instrumented coolant channels) and a pressure tap. Another pressure tap was located on the injector face, as shown in figure 2, to measure combustion pressure at that point.

The number of instrumentation planes was increased to 15 for thrust chamber 2. The locations of these stations are shown in figure 1 and are 1.0 inch apart on the coolant flow path, with station XI at the nozzle throat. The larger number of stations was to provide increased data resolution and to provide data somewhat nearer the chamber ends than was obtained with chamber 1. To avoid exceeding data recording capacity, the number of thermocouples was limited to four at each station, along with a total of eight coolant channel static-pressure taps. The instrument array for each station is shown in figure 3. On the designated station plane in this chamber were grouped thermocouples 2, 3, and 4, direct counterparts of the same-numbered instruments of thrust chamber 1. Thermocouple 5 was located 0.12 inch upstream on the coolant flow path and the coolant static pressure tap was 0.19 inch downstream at odd-numbered stations only. Here as with thrust chamber 1, the instrumented coolant channel containing the pressure taps is called channel 1, while the other instrumented channel located diametrically opposite, channel 2, has no taps. Other chamber and injector instrumentation was identical to that of chamber 1.

The fine thermocouple leads from the thrust chamber (exclusive of the manifold instrumentation) were connected to terminal strips attached to the outer chamber wrap. This may be seen in figure 4. From the terminal strips, heavier alloy leads were connected to low-resistance, multiple-connector, quick-disconnect-type plugs mounted off the chamber surface. Also shown in figure 4, the coolant static-pressure tap tubes were attached to fitings mounted on a bracket near the chamber surface. The pressure transducers were attached as closely as possible to the thrust chamber to keep the length of the tubes to a minimum.

Propellant Flowmetering and Controls

The liquid hydrogen and liquid fluorine flow systems are shown schematically in figure 5, as are the thrust-chamber operating controls. The entire system is quite similar to that described in reference 1. In brief, the hydrogen weight-flow rate was preset into

the electrical servocontroller, as was the desired fuel weight fraction. The controller was equipped to accommodate several sequential running conditions, if desired. After a brief hydrogen lead period to fill the chamber's coolant channels, the fluorine flow rate rose to satisfy the desired running condition. Any necessary correction of either propellant's weight-flow rate during a run was made by controller adjustment of the fire valve settings. Fire valve position "hunting" was minimized by not incorporating a chamber pressure control. This simplification was of course at the expense of small but essentially steady-state deviations from desired chamber pressure. Both propellants were metered with venturi flowmeters.

Primary malfunction-sensing devices were monitoring sensors on both hydrogen and fluorine flow rates and on combustion chamber pressure. Significant off-condition values of these quantities would initiate rapid shutdown of the apparatus.

Experimental Facility

The main elements of the facility used in this study appear schematically in figure 5. The installation is thoroughly described in reference 1. One of the important features is the liquid nitrogen bath in which the liquid fluorine tank and all but a few inches of the fluorine supply line to the thrust chamber were submerged. This kept the fluorine in its liquid state, since the boiling temperature of nitrogen is below that of fluorine. The liquid hydrogen tank was insulated with a vacuum jacket, and the supply line had a wrap of aluminum-foil-covered asbestos tape. Also worthy of note is the exhaust-gas scrubber, in which the products of combustion were deluged with several thousand gallons of water spray per minute to remove toxic products and to cool and quiet and remainder of the gas before it was discharged to the atmosphere.

A modification made in the facility for this investigation was the addition of a zero-flow, straight-tube ejector through which the thrust chambers exhausted to the scrubber system. The ejector was designed by means of the methods indicated in reference 10 and ensured that the chamber nozzles would flow full during operation. Without an ejector, the nozzles would experience flow separation, since internal pressures were well below atmospheric (as low as 2.34 psia) at the conditions of this study.

EXPERIMENTAL PROCEDURES AND MEASUREMENTS

Thrust-Chamber Operation

Combustion, propellant injection, and coolant pressures usually reached essentially

steady-state values in less than 2 seconds after the fluorine fire valve was opened. Since the thrust chamber was constructed of relatively thin walls, the midwall temperatures (thermocouples 2 and 4 in fig. 3) reached their levels of least variation rapidly as well, typically within 7 seconds. The coolant temperatures (thermocouple 3 in fig. 3), particularly those nearest the coolant inlet manifold, however, rose to their steady-state level more slowly, taking up to 10 or 11 seconds in some cases. In a typical 15- to 18-second run (total time), a period of at least 6 consecutive seconds could be selected which was suitable for steady-state study. During that period, it is estimated that the maximum deviation from a mean value of any of the temperatures or pressures used was about ±5 percent, with the bulk of the data displaying less deviation than that. Temperatures and pressures recorded during the nominal steady-state period for a particular run were not exceeded at other points in the run.

Data Recording

The experimental data for this study were all tape recorded in digital form at a basic sampling rate of 4000 readings per second and were visually inspected during recording and by playback later with a sustained-trace oscilloscope. In this way, the nominal steady-state period was readily identified. In addition, several quantities were simultaneously recorded on strip-chart recorders for continuous monitoring during operation. These quantities included combustion pressure, flowmeter readings, and fire valve position indications.

The magnetic tape containing the data was ultimately read into a digital computer which converted the recorded impulses into the appropriate temperature and pressure values. To keep the quantity of data to be used within reasonable limits, a convenient "report time interval" was selected in which all individual instrument readings were averaged and reported as a single reading for each instrument for the duration of the period. A report time interval of 0.48 seconds was selected for this investigation. Since the number of instrument recording units used for thrust chamber 1 was 128, each report time interval included 15 readings of each instrument; while for chamber 2's 160-instrument recording units, 12 readings of each sensor were included. The averaging of the readings within the report time intervals helped reduce the effects of random extraneous noise signals. Predictable 60-cycle noise was effectively minimized by system isolation during operation.

The computer produced a plot of each of the instrument readings by report time intervals to confirm the nominal steady-state period selection. In addition, it supplied an overall average for all selected steady-state report time intervals for each instrument as a single summary report.

Experimental Measurements

Operating conditions. - Table III presents a summary of the operating conditions of each of the runs used in this study, averaged over the steady-state period of the run. The combustion pressure and injector pressure drops were measured at about half scale with oversized commerical transducers with a maximum nonlinearity of 1 percent at full scale. The flowmeter pressure drops were measured with similar transducers at nearly full scale. The liquid hydrogen temperature at the flowmeter was measured by means of a carbon resistor thermometer with an estimated error of within $\pm 0.5^{\circ}$ R.

Some variation from desired combustion pressure and fuel mixture for each of the runs used in this study is shown in table III. The combustion pressure is off about 10 pounds per square inch from the intended value for run 8, to point out the worst case. These variations came about in part because the control system did not include a combustion pressure control loop, as described in the section Propellant Flowmetering and Controls. The thermodynamic and transport properties involved in the heat-transfer studies to be described, however, are not particularly sensitive to small changes in pressure or fuel mixture. As a consequence, the properties used in this study are as listed in table II, and are not computed for each run's specific operating conditions.

Coolant channel midwall temperatures. - The steady-state averaged midwall temperatures $T_{w,m}$ used for all the runs of this study are shown in figure 6 and are tabulated in table IV. Thermocouple 4, described earlier and shown in figure 3, was used for $T_{w,m}$ to the exclusion of thermocouple 2, since the former instrument consistently indicated a higher and therefore more conservative temperature from a design standpoint. This temperature pattern is discussed and analyzed in reference 11. Furthermore, a few times thermocouple 2 exhibited a tendency to migrate toward the hot-gas wall surface from 0.002 to 0.005 inch during fabrication brazing cycles. Because of this, thermocouple 4 was judged to be the more valid of the two instruments for the purpose of this study.

Figure 6 presents $T_{w,m}$ data for coolant channel 1 for both chambers 1 and 2, but data for channel 2 for chamber 2 only. At most stations, thermocouple 4 in channel 2 of chamber 1 was damaged in fabrication, and the readings of those few useful ones are tabulated in table V. Where data points do not exist in figure 6, conservative estimates were supplied on the basis of observed trends of more complete data such as that of run 9, channel 2, and run 10, channel 2.

A discussion of the accuracy of the $T_{w,m}$ measurements must include several points. First, the very presence of the relatively large thermocouple assembly (0.020 in. diam.) in the 0.022-inch-thick wall indicates an obvious temperature distortion effect. Also, the between-channel grooves tended to fill somewhat more with braze material at the instrument stations than elsewhere, because of the method of thermocouple installa-

tion (see appendix B). The complete effects of these conditions are unresolved, but a compensating factor is that the sensing portion of the thermocouples were solid balls (see fig. 3) of mostly type 304 stainless steel, as was the channel material. Further, the instruments were brazed in place with material having essentially the same thermal conductivity as the channel material. Therefore, the temperature distortion effect was diminished at the sensing junction. Additionally, as will be seen, the subsequent calculations of this study are not particularly sensitive to relatively small wall temperature errors.

A less important consideration is the error which may come about because the actual thermocouple junction was Chromel to stainless steel to Alumel. Depending on the orientation of the junction with the heat flow path through the channel wall, calculations show an error of about $\pm 30^{\circ}$ R may result. Again, an error of this magnitude would not seriously affect the calculations to be developed later in this study.

Representative tests indicated the brazing and heat-treating cycles in the chamber fabrication process described in appendix A, while sometimes damaging the thermocouple assemblies structurally, did not alter their calibration significantly.

Great care was taken to place the thermocouple sensing junction in position accurately and to provide a thin, smooth braze seal over the instruments to keep measurement errors from these sources to a minimum. It is felt that, considering all factors, the thermocouples indicated the correct wall temperatures within $\pm 100^{\circ}$ R.

Coolant temperatures. - Thermocouple 3 shown in figure 3 was used to measure the averaged steady-state coolant temperature profiles shown in figure 7 and tabulated in table IV. As described earlier, these 0.020-inch-diameter copper-constantan instruments were inserted about 0.030 inch into the coolant stream on the channel centerline. Probably in part because of minor instrument placement differences, the data scatter was considerable in thrust chamber 1, particularly in channel 2. Those curves which were fitted through just a few data points or through scattered ones were shaped as suggested by the general contours of the curves developed in figure 7(c) for the 18 percent fuel weight fraction condition, where the data were considerably more complete. Additional coolant temperature curve shape information was supplied by the data of a number of runs which are not included in this study because their midwall temperature data was not complete enough to be useful. The portion of the curve at the coolant inlet manifold end of the thrust chamber is simply a convenient shape to the known coolant inlet temperature level. The curve section at the injector end of the chamber was fitted to end the curve in the region indicated by the injector manifold thermocouple values. This curve fitting appears to be justified by the data of figure 7(c), where data exists relatively near the injector manifold. The rather wide scatter in the injector manifold temperatures is in large part caused by the thermocouples not being in similar positions in the injector coolant passages. Because of interfering accessory equipment and injector at-

taching hardware, each thermocouple was somewhat differently placed relative to the fluorine tubes and the ends of coolant channels.

An evaluation of the conduction error for thermocouple 3 indicates a possible error of about 5° to 9° R at stations near the coolant inlet manifold where the largest temperature differences between coolant and chamber wrap occur. At locations further downstream relative to coolant flow where the temperature difference is less, the indicated possible errors are nearly negligible.

Other temperatures. - Although not used directly in this study, table V includes steady-state data obtained from thermocouples 2 and 5 (see fig. 3) for comparison and reference. Data from thermocouple 1 was not included in table V, since uneven braze covering of this between-channel thermocouple caused the data to scatter so much that it was not usable. The data of thermocouple 7 were quite similar to that of thermocouple 5 (both chamber wrap surface temperature sensors) and so were omitted from the table. The four values measured by thermocouple 6 in chamber 1 were essentially the same as those of thermocouple 3 at the same station and were also omitted from tabulation.

Coolant pressures. - Figure 8 presents coolant static-pressure profiles for all the runs of this study, averaged over the steady-state periods. This data is presented in table IV and is considerably more complete than the other thrust-chamber values. Note that the hydrogen is well below its critical pressure (about 188 psia) through the entire coolant flow path in the thrust chamber. With the exception of the first, and sometimes second, instrument station downstream from the coolant inlet manifold, the pressure data were satisfactorily stable. The first stations, however, generally exhibited quite high noise levels, probably reflecting the coolant's phase change in the nearby channel entrance region. As a result, the noisy data from the first two stations may be in error, and except for the display in figure 8, will be used subsequently in this study only to provide an approximate pressure for coolant enthalpy determinations. An attempt was made to keep the readings about midrange on the transducers to keep the indicated error within 1 percent of full-scale value.

CALCULATIONS AND RESULTS

Thrust-Chamber Performance

Theoretical values of the characteristic exhaust velocity c* were computed by the methods described in references 5 and 6. The values at 60-pound-per-square-inch combustion pressure and 12, 15, and 18 percent hydrogen by weight are given in table II, along with an equation for corrections for small deviations in pressure. For runs deviating a small amount from the specified fuel weight fractions, theoretical values of c*

were determined by interpolation.

Experimental values of c* were computed for the steady-state period of each run by the relation

$$c^* = \frac{p_c A_{tht} g}{12\left(w_{H_2} + w_{F_2}\right)}$$

(All symbols are defined in appendix B.) The combustion pressure was measured at the injector face and therefore was corrected to the true combustion pressure (at nozzle inlet) by the method of reference 3.

Table III presents a summary of the characteristic velocity efficiencies, based on equilibrium composition, for each of the runs of this study, averaged over the steady-state period of the run. This efficiency is defined as

$$\eta_{c^*} = \frac{c^*_{act}}{c^*_{theo}} \times 100$$

Partly because the experimental run values of table III so closely approximate 100 percent, all the calculations used in this study are based on the equilibrium assumption. As was stated earlier, this assumption is in agreement with the findings reported in reference 1, 3, and 4.

For a system in which the c* efficiency is significantly less than 100 percent, the theoretical combustion temperature must be revised downward. As was stated earlier, however, the values of η_{c^*} shown in table III are all essentially 100 percent (within the limits of experimental accuracy). Therefore, no combustion temperature corrections were made for the purposes of this study.

Heat Flux Calculations

Localized heat flux values were determined on the basis of coolant enthalpy increase. Referring to figure 1, the change in coolant temperature and pressure between two successive instrumentation planes gave rise to an increase in enthalpy which was computed using the properties of reference 8. Specifically, corresponding station values of T_l for the two channels for each run were read from figure 7 and averaged. The values of p_l were obtained from figure 8. The governing equation, applied between instrument stations, may be written

$$n[Q]_{n+1} = w_{H_2,\,T_n}[\Delta i_l]_{n+1}$$

where

$$\Delta i_l = f(T_{l,\,s}, \Delta T_{l,\,s}, p_l, \Delta p_l)$$

Although the instrumentation used in this study did not define temperature profiles across the channels, it was assumed that the measured values represented mean effective temperatures. Since the maximum computed Mach number for the coolant was about 0.4, the measured temperature was considered to be free stream static temperature for the calculations of this study.

The coolant pressure profile measured along channel 1 was assumed to apply to channel 2 as well in these and following calculations. The probable error in enthalpy determination due to this assumption is acceptably small, since enthalpy is primarily a function of temperature for the coolant at these conditions.

The resulting values of $Q/A_g = q_g$ were assigned to points midway between instrumentation planes, and connecting curves were plotted. The quantity A_g is the thrust-chamber inside perimeter at the instrumentation station multiplied by the surface distance between stations. These q_g values are presented in figure 9. Note that the heat flux peaked near the throat position for all the runs studied and that relatively good agreement occurred for runs of similar conditions. The contribution by radiation to the total heat flux to the thrust-chamber wall was estimated to be about 5 percent of the total, and therefore no attempt to deal with it separately was made in this study. As a consequence, all determinations pertaining to heat transfer to the wall in this investigation consider the entire q_g to be convective. Also, longitudinal conduction in the chamber walls was neglected, since temperature gradients in that direction were very much smaller than in the radial direction. Finally, since the natural convection heat-transfer coefficient between the thrust-chamber wire wrap and the surrounding air was very much smaller than the other coefficients considered in this study, that heat transfer was also neglected.

Coolant Flow Distribution

It was necessary to determine a weight-flow rate specific to each coolant channel in order to determine the heat-transfer correlation equation constants ($\bar{K}_l$ and $\bar{K}_g$), as will be seen in the section Heat-Transfer Correlations. While the channels were fabricated as nearly alike as possible, their heights varied significantly in the completed chamber assembly, as may be seen from the tabulated dimensions of table I. The nonuni-

formity, along with some differential instrument blockage, caused a circumferential unevenness in coolant channel weight-flow rates. This unevenness precluded the possibility of using an average weight-flow rate for the channels. Flowmetering of the individual instrumented channels during operation was not considered practical because of the very small flow rates and the mechanical complexity involved.

A basic assumption made to facilitate the coolant weight-flow rate distribution was that the heat flux at any plane perpendicular to the chamber centerline was circumferentially uniform. On examination, this assumption appears valid since even if wall temperatures were to vary by several hundred degrees around a chamber at a plane, the percentage of heat flux variation would still be quite small, because of the relatively high combustion temperature. It is noted that the data for chamber 2 (fig. 6(c)) indicates relatively similar wall temperatures at its two diametrically opposed instrument channels. Furthermore, careful examination of the chambers after each firing indicated no local "hot spots" or areas where significantly higher or lower temperatures resulted in differential chamber discoloration or damage.

By utilizing the uniform heat flux assumption described, the coolant weight-flow distribution for the two instrumented coolant channels on each chamber was determined on the basis of relative enthalpy increase. The coolant enthalpy increase in each instrumented channel was computed from the uniform conditions at the coolant inlet manifold by using the channel instrument station nearest the injector as an end point. Since the heat flow into each channel was assumed identical, only the weight-flow rates must vary. Then, for any specific run,

$$\left[w_{H_2}\right]_{ch1} = {}_{in}\left[\frac{Q/72}{\Delta i_l}\right]_{A \text{ or } I,\, ch1}$$

and

$$\left[w_{H_2}\right]_{ch2} = {}_{in}\left[\frac{Q/72}{\Delta i_l}\right]_{A \text{ or } I,\, ch2}$$

The weight-flow rate distributions calculated in this manner, along with a percentage comparison, appear in table VI.

Heat-Transfer Coefficients

Combustion gas to wall. - Reference 12 recommends that the gas-to-wall heat-

transfer coefficient be defined on the basis of an enthalpy difference when a variable specific heat is involved. This is written as

$$h_{g,i} = \frac{q_g}{i_{g,aw} - i_{g,w}}$$

where

$$i_{g,aw} = i_{g,s} + Pr_{g,i^*}^{0.333}(i_{g,t} - i_{g,s})$$

and Pr_{g,i^*} is based on "reference enthalpy" i_g^* where

$$i_g^* = 0.5(i_{g,s} + i_{g,w}) + 0.22\ Pr_{g,i^*}^{0.333}(i_{g,t} - i_{g,s})$$

(Note that the units of $h_{g,i}$ are (lb)/(sec)(sq in.).) In order to evaluate $i_{g,w}$, the gas-side wall surface temperature is required. If the thermocouple measuring $T_{w,m}$ is embedded at about midwall (see appendix A) and if the local q_g from the curves of figure 9 is known, the required surface temperature is found from the relation

$$T_{g,w} = T_{w,m} + \frac{q_g b_w}{2k_w}$$

where

$$k_w = f(T_{w,m})$$

The computed values of local $h_{g,i}$ are shown plotted in figure 10. While level differences exist between the curves of the three fuel weight fractions, general trends appear to be similar, with peak values occurring near the nozzle throat position.

Wall to coolant. - The coolant-side heat-transfer coefficient in this study is defined as

$$h_l = \frac{q_g}{T_{w,l} - T_{l,s}}$$

where the units of h_l are Btu per second per square inch per ^{o}R. The same assumptions as earlier are used to determine the value of $T_{w,l}$ from the expression

$$T_{w,l} = T_{w,m} - \frac{q_g b_w}{2k_w}$$

where again

$$k_w = f(T_{w,m})$$

Implicit here is the assumption that the heat flux from wall to coolant is equal to that from combustion gas to wall, although the inside channel heated surface width is less than the corresponding gas-side surface by about two channel wall thicknesses because of the presence of radial webs. The fluxes were assumed to be equal to afford a convenient and conservative allowance for some transfer of heat to the coolant from the radial webs of the channels. The coefficients determined for each instrumentation plane are shown plotted in figures 11. General similarities among the three conditions are in evidence, although some specific differences in curve shapes exist.

It is important to note that all the data and calculated curves presented to this point are specific to the particular apparatus configuration and conditions studied here. They should not, of course, be considered in any way general or predictive of other tests. This information has been presented as background for the more general material that follows these sections.

Heat-Transfer Correlations

Combustion gas to wall. - In addition to recommending that the gas-side heat-transfer coefficient be defined as a function of enthalpy difference, reference 12 also indicates the properties in a correlating equation should be introduced on an enthalpy basis. This "reference enthalpy" is defined by an equation noted earlier, that is,

$$i_g^* = 0.5(i_{g,s} + i_{g,w}) + 0.22\ Pr_{g,i^*}^{0.333}(i_{g,t} - i_{g,s})$$

Reference 13 indicates that the heat transfer through a turbulent boundary layer can be approximated quite closely by a dimensionless number correlation for fully developed turbulent flow, even though fully developed turbulent flow is not necessarily assumed.

As a consequence, a correlating equation of the form

$$Nu_{g,\,i^*} = \overline{K}_g Re_{g,\,i^*}^{0.8} Pr_{g,\,i^*}^{0.333}$$

will be utilized in this portion of the study. In more basic symbols, this equation may be written

$$\frac{h_{g,\,i}(c_p)_{g,\,i^*} D_g}{k_{g,\,i^*}} = \overline{K}_g \left(\frac{G_g D_g}{\mu_{g,\,i^*}} \frac{T_{g,\,s}}{T_{g,\,i^*}} \right)^{0.8} \left(\frac{c_p \mu}{k} \right)_{g,\,i^*}^{0.333}$$

Use of the equation in this form implies the familiar assumption of constant static pressure through a boundary layer. Also implied is the assumption that the change in molecular weight is small between stream static and reference enthalpy conditions. Indeed, the calculated maximum difference in molecular weight between the two conditions is about 2 percent. The quantity $\overline{K}_g$ is a variable along a varying cross-sectional-area flow path and was determined for local regions of the thrust chambers.

Figures 12(a), (b), and (c) present the local calculated values of $\overline{K}_g$ along the length of the thrust chambers for the three fuel weight fractions studied here. Examination of these figures indicates the two injector types used in this study did not discernibly affect the shapes or levels of the curves. The curves show a dip to a range of about 0.013 to about 0.019 (average) at approximately the nozzle throat location. If this level is compared to the commonly used tube flow value of 0.023, the experimental throat value is about 20 to 40 percent low and is in agreement with the 0.023 value only in the combustion chamber region several inches downstream from the injector face. The quantity $\overline{K}_g$ increases to a maximum of about 0.023 about 6 to 7 inches from the injector face, possibly indicating that the gas temperature did not reach its full equilibrium level before reaching that plane. This effect is also indicated in figure 6 where peak values of the midwall temperature occur at about 6 inches from the injector. Appearing in figure 12(d) is a summary of the average lines of figures 12(a), (b), and (c) for convenient comparison. Generally good agreement between these average lines is apparent. The effect on the shapes of these curves due to the different propellant mixtures used here is apparently small. It is pertinent here to point out that the ratio of gas static temperature to gas-side wall temperature for all the stations in the thrust chambers of this study were fairly uniform and moderate, ranging from about 3 to about 6. Worthy of note here is the relatively good $\overline{K}_g$ agreement at the throat and combustion chamber, particularly for the 15 and 18 percent runs, with the similarly determined correlation equation coefficients of reference 14. Reference 14 reports on a heat-transfer study conducted with a thick wall, uncooled thrust

chamber using the propellant combination hydrogen and oxygen at combustion pressures from 150 to 1000 pounds per square inch absolute.

The values of $\overline{K}_g$ in conjunction with its equation presented in this report for the various thrust chamber locations and conditions noted are valid only when used with the chemical equilibrium properties listed in table II and/or the indicated references. If a similar thrust chamber is to be designed or evaluated by the described equation and localized $\overline{K}_g$ values, these properties or calculation procedures must be used. Experience has shown that the value of $\overline{K}_g$ may be shifted by as much as 50 percent simply by the use of other available property values. The properties used in this study are considered by Lewis to be the most accurate presently available.

Wall to coolant. - It was assumed that the heat transfer between coolant channel walls and coolant could be approximated by means of a tubular fully developed turbulent flow correlation form, specifically,

$$Nu_{l,T_f} = \overline{K}_l Re_{l,T_f}^{0.8} Pr_{l,T_f}^{0.333}$$

where the properties are introduced at a coolant film temperature T_f defined as

$$T_f = 0.5(T_{w,l} + T_{l,s})$$

More basically, the correlating equation is written

$$\frac{h_{l,T_f} D_l}{k_{l,T_f}} = \overline{K}_l \left(\frac{G_l D_l}{\mu_{l,T_f}} \frac{\rho_{l,T_f}}{\rho_{l,T_s}} \right)^{0.8} \left(\frac{c_p \mu}{k} \right)_{l,T_f}^{0.333}$$

The quantity $\overline{K}_l$ was, in a manner similar to the treatment of $\overline{K}_g$, determined for local regions along the variable-area flow path of the coolant channels. Comparison of the run conditions and coolant channel configurations for the thrust chambers of this study and those of reference 15 indicate that the local effects on coolant heat transfer due to channel curvature do not appear to be significant, and they were neglected.

It was noted that the computed local values of $\overline{K}_l$ (see figs. 13(a), (b), and (c)) exhibit quite high levels (approaching 0.06) near the coolant inlet manifold and extending to near the nozzle throat, as compared to the commonly used value of 0.023. An examination of the average values of the ratio of coolant-side wall temperature to coolant static temperature, shown plotted in figure 14, reveals a marked similarity to the trends of the $\overline{K}_l$ curves, indicating a possible strong relation. Such a relation has been noted in

reference 16 where a parameter similar to $\overline{K}_l$ was found to have a much higher value at higher levels of wall-to-coolant bulk temperature ratio (up to 4.43) than at lower levels for gaseous hydrogen flowing in an electrically heated tube. Reference 16 suggests that because of the high wall-to-coolant bulk temperature ratios near the coolant channel inlet, the establishment of a fully developed temperature profile across the channel is delayed. This lengthens the entrance effect and results in higher-than-anticipated values of $\overline{K}_l$ in that region.

When the data of the present study was reexamined by means of a correlating equation containing a wall-to-coolant temperature ratio in a form found useful (by Robert C. Hendricks of the Lewis Research Center) with some other data for moderate (to about 5) $T_{w,l}/T_l$ ratios, specifically,

$$\frac{h_{l,T_f} D_l}{k_{l,T_f}} = \overline{K}_l \left(\frac{G_l D_l}{\mu_{l,T_f}} \frac{\rho_{l,T_f}}{\rho_{l,T_s}} \right)^{0.8} \left(\frac{c_p \mu}{k} \right)_{l,T_f}^{0.333} \left[1 + 0.014 \left(\frac{T_{w,l}}{T_{l,s}} \right)^{1.5} \right]$$

the total data correlation (along the entire length of the thrust chamber) was not improved significantly. A considerably stronger $T_{w,l}/T_{l,s}$-dependent relation is apparently required for good total data correlation in the present study. Another possible explanation for the relatively high values of $\overline{K}_l$ near the coolant inlet manifold is that the hydrogen, being in a near-critical condition, may still contain some liquid-phase droplets, probably in the 1- to 10-micron (mist flow) size range. The small liquid particles would cause the experimental heat-transfer coefficients to be higher than those predicted by means of a film temperature correlation procedure as discussed in reference 17. Without additional information, a reasonable suggestion would be to provide allowance for a higher-than-normal value for $\overline{K}_l$ in a near-critical region or near an entrance region with wall-to-coolant bulk temperature ratios greater than about 5.

The values of $\overline{K}_l$ reduce from higher levels to about 0.025 (average) near the nozzle throat. Considerable variation of the curves is in evidence (see figs. 13(a), (b), and (c)) in thrust chamber 1 at a point about 6 inches from the injector face. This is due to the very high midwall temperatures measured at that location (refer to figs. 6(a) and (b)). The quantity $\overline{K}_l$ is relatively more sensitive to wall temperature than is $\overline{K}_g$ because of the great difference in the temperature differences between gas to wall and wall to coolant. It was felt that the wall thermocouple at station B in thrust chamber 1 consistently read somewhat higher than the actual temperature at that point (see figs. 6(a) and (b)). No effect on these curves due to the two injector types used is discernible. Figure 13(d) presents a summary of the averaged curves of figures 13(a), (b), and (c) for convenient comparison. The $\overline{K}_l$ curve for the 18 percent hydrogen fuel weight fraction in figure 13(d),

possibly idealized to a straight horizontal line through the average level (about 0.025), appears to reasonably represent the function for the throat and combustion zone portions of the thrust chamber. As with the combustion gas-to-wall heat-transfer process, the shapes of the curves of figure 13(d) are not significantly affected by the different propellant mixtures used in this study.

If the $\overline{K}_l$ information presented here is used for design or evaluation purposes for similar thrust-chamber systems, use of the hydrogen properties utilized in this study is urged.

Use of correlation values. - The anticipated use of the results of this investigation is to provide the designer with information to help him specify the cooling system configuration of a regeneratively cooled rocket engine thrust chamber. In addition, the same information should also help to evaluate an existing system for off-design operation. It is urged that such designers examine the criticality of their design values, such as wall temperatures, heat fluxes, and others, in view of the bands of data scatter from which the determinations of this study were made. On the basis of this examination, then, desirably conservative designs or evaluations can be made. A further point should be made that it has been shown (ref. 18) that gaseous-hydrogen heat-transfer correlations extrapolated to conditions much different from their determining experimental data can result in questionable results. These discrepancies are particularly significant at higher surface temperatures or very low bulk temperatures.

Coolant Pressure-Loss Study

The total coolant pressure loss in a channel is the sum of the friction and momentum losses. For variable cross-sectional-area, diabatic tube flow with losses, it may be shown that between two stations, n and n + 1, the momentum pressure loss may be written

$$n\left[\Delta p_l, M\right]_{n+1} = \frac{w_l^2}{g\overline{A}_l}\left(\frac{1}{\rho_{l,\,n+1} A_{l,\,n+1}} - \frac{1}{\rho_{l,\,n} A_{l,\,n}}\right)$$

The friction pressure loss then is identified as

$$n\left[\Delta p_l, f\right]_{n+1} = n\left[\Delta p_l, T\right]_{n+1} - n\left[\Delta p_l, M\right]_{n+1}$$

The Fanning friction factor f, a convenient parameter in frictional flow studies, is determined from the relation

$$f_l = \frac{n\left[\Delta p_{l,f}\right]_{n+1} g\bar{D}_l\bar{\rho}_l}{2\bar{G}_l^2 l}$$

By referring to the coolant pressure data presented in figure 8, the Fanning friction factor was computed for each usable interstation length of coolant passage. The resulting values are shown plotted in figure 15. Also shown in figure 15 is a modified form of an equation developed by Koo for the Fanning friction factor in long, smooth tubes (ref. 19). While the original Koo relation based the viscosity on the coolant bulk temperature, the equation used in this study based the viscosity on film temperature to be consistent with the coolant-side heat-transfer correlations considered here. The modified Koo equation was written

$$f'_{l,\,Koo} = 0.00140 + 0.125\left(\frac{\bar{G}_l\bar{D}_l}{\bar{\mu}_{l,T_f}}\right)^{-0.32}$$

Note that the Koo equation line passes through essentially the lower portion of the computed friction factor points of figure 15. It may be speculated that, since the thrust-chamber coolant passages are considerably more rough than the conditions for which the Koo equation was developed, the bulk of the friction factor data of this study could be expected to lie above the Koo line. Therefore, the results of this study indicate a useful approximation of the Fanning fraction factor in coolant channels and for flow conditions similar to those examined here to be about 25 percent higher than those predicted by the modified form of the Koo equation.

SUMMARY OF RESULTS

An experimental investigation was conducted to determine localized gas-to-wall and wall-to-coolant heat-transfer and coolant pressure-loss characteristics in regeneratively cooled hydrogen-fluorine rocket engine thrust chambers. The chambers had nozzle throat design diameters of 3.910 inches and design contraction and expansion ratios of 1.897 and 3.679, respectively; propellant mixtures were about 12, 15, and 18 percent hydrogen by weight, and the combustion pressure was about 60 pounds per square inch absolute. A

summary of the results is as follows:

1. The combustion-gas-to-wall heat transfer for the conditions of this study appears to be adequately approximated by the relation

$$Nu_{g,\,i*} = \overline{K}_g Re_{g,\,i*}^{0.8} Pr_{g,\,i*}^{0.333}$$

where $Nu_{g,\,i*}$, $Re_{g,\,i*}$, and $Pr_{g,\,i*}$ are the Nusselt, Reynolds, and Prandtl numbers, respectively, based on reference enthalpy and where $\overline{K}_g$ is a coefficient depending on location in the thrust chamber. The quantity $\overline{K}_g$ varies throughout the chamber, from a maximum average of 0.023 in the combustion region to a minimum average of 0.013 at the nozzle throat.

2. The wall-to-coolant heat-transfer for the conditions of this study appears to be satisfactorily approximated locally within the coolant passages for moderate wall-to-coolant bulk temperature ratios (up to about 5) by the relation

$$Nu_{l,\,T_f} = \overline{K}_l Re_{l,\,T_f}^{0.8} Pr_{l,\,T_f}^{0.333}$$

where $Nu_{l,\,T_f}$, $Re_{l,\,T_f}$, and $Pr_{l,\,T_f}$ are Nusselt, Reynolds, and Prandtl numbers, respectively, all based on coolant film temperature. For the coolant condition regime described, the coefficient $\overline{K}_l$ is reasonably approximated by the value 0.025.

3. For relatively high wall-to-coolant bulk temperature ratios (above about 5), particularly near an entrance region, and/or for coolant conditions near critical, the coolant-side correlation equation shown previously is not sufficient. A wall-to-coolant temperature ratio correction and/or a two-phase flow correction is apparently required.

4. No effects of the two coaxial injector types used in this study are evident on the values of $\overline{K}_g$ and $\overline{K}_l$ determined.

5. No important effects of the three propellant mixtures used in this study are evident on the values of $\overline{K}_g$ and $\overline{K}_l$ determined.

6. The coolant friction pressure loss for coolant channels and flow conditions similar to those examined in this study is approximately described by means of a Fanning friction factor which is 25 percent higher than that predicted by a modified form of the Koo equation for long, smooth tubes.

Lewis Research Center,
National Aeronautics and Space Administration,
Cleveland, Ohio, March 22, 1967,
128-31-06-01-22.

APPENDIX A

INSTRUMENTED THRUST-CHAMBER FABRICATION

Fabrication procedures for the thrust chambers used in this study were significantly different from those described in an earlier investigation (ref. 1) and merit special attention here. Many of these changes, some of which required extensive development, came about because of the additional complexities imposed by the instrumentation installation.

Channel Preparation and Assembly

Individual coolant channels conforming to thrust-chamber contour were formed from 0.022-inch-thick type 304 stainless steel, with webs purposely left somewhat longer than the final intended dimension. Those channels which were to contain thermocouples within their walls were appropriately slotted on the channel bottom and one or both webs to a depth of 0.020 inch. Care was taken to ensure that the necessary matching slots in the webs of adjacent channels alined. Views of a slotted channel set are shown in figure 16.

After slotting, the channels were cleaned and then assembled in their proper positions on a forming mandrel. There, held together by clamps and bands, the channel webs were electrically spot-welded together. Because of channel fabricating tolerances, it occasionally happened that full-length shimming between adjacent webs was required for the 72 channels to span the mandrel's circumference. In these instances, type 304 stainless-steel shims, both tapered or untapered as required, were spaced evenly around the assembly, avoiding instrument-bearing channels and adjacent locations. Maximum shimming between any two adjacent channels was 0.009 inch.

Following channel assembly, short lengths of stainless-steel tubing to be used later as drilling guides were inserted into the radial web slots with fitting tolerances such that they would braze to the channels in a subsequent operation. The inside of these tubes and the slots on the channel bottoms were treated with a metal oxide slurry to prevent braze material from flowing into them.

First Wrapping and Brazing

The prepared thrust chamber assembly was next placed on a brazing mandrel which had been ceramic-coated to prevent its attachment to the chamber.

With the mandrel-mounted thrust chamber in place in a lathe, a wire wrapping was applied. Starting at the throat section and moving each way toward the chamber ends, a

1/16-inch-diameter type 308 stainless-steel round-section wire was wrapped in high tension over the entire chamber to pull it into intimate contact with the mandrel to assure good pattern conformity. Brazing wires of 94 percent copper and 6 percent nickel were applied between and under the stainless-steel wire wraps. The entire assembly was then placed in a vacuum furnace where it was brazed at about 2075° F, with the thrust chamber in a nozzle-down position.

Coolant Channel Machining

After brazing, the thrust chamber was removed from the mandrel and all surfaces with the exception of channel interiors, were sealed with epoxy resin. The coolant channels were then filled with a low-melting-temperature (about 200° F) metal, after being treated with hot mineral oil to assure good subsequent cleaning.

The thrust chamber was next placed on the forming mandrel and lathe-turned to the proper coolant channel height profile by means of a template and pantograph attachment. The wire wrapping was of course machined away in the process. The soft metal in the channels prevented the webs from being deformed during machining.

When proper dimensions were achieved, the thrust chamber was steamed to remove the soft metal, the machined surfaces were deburred, and the entire unit was carefully cleaned.

Second Wrapping and Brazing

Again, the thrust chamber was placed on the ceramic-coated brazing mandrel. The assembly was then placed in a lathe for high-tension wire-wrapping the thrust chamber as before. This time, however, type AM 350 stainless-steel wire was used. The wire was roller-flattened during wrapping from 1/16-inch-diameter round section to a 0.040-inch-thick, almost-rectangular section. This operation is shown in figure 17. A brazing slurry of pure copper suspended in acryloid cement and acetone was brush-applied over the entire outside surface, and the unit vacuum-brazed at about 2010° F.

After this brazing cycle and every subsequent cycle, a radiographic examination of the thrust chamber was performed to locate braze-blocked (or partially blocked) coolant channels or other imperfections if they existed.

Flange Fitting and Brazing

The injector flange and combination nozzle flange-manifold assembly, both stainless

steel, were fitted to the thrust chamber during the next step in the fabrication procedure. Flange attachment was accomplished by vacuum-brazing with a material consisting of 35 percent gold, 62 percent copper, and 3 percent nickel. This material, in wire form, was placed in machined surface-matching grooves in the flanges. Brazing was accomplished at a temperature of about 1925° F.

Instrument Installation

To prepare the thrust chamber to receive the thermocouples, a small right-angle drill driving a 0.024-inch-diameter bit was used inside the chamber to drill outward through the wire wrapping, using the embedded stainless-steel tubes described earlier as guides. Caution was exercised to avoid puncturing the coolant channel walls. After all traces of the brazing inhibitor material were removed from the thermocouple-receiving slots and tubes, preshaped thermocouples were inserted into position from the inside of the thrust chamber.

To hold the thermocouples firmly in place for brazing, they were bent over at the thrust-chamber outside surface, allowing a small radius, and were held down with small nichrome strips electrically welded to the surface. Surface thermocouples were positioned and fixed in place and the coolant thermocouples were inserted into drilled holes to the appropriate depth and similarly anchored. The exposed portions of the thermocouple leads were protected with brazing inhibitor material and covered with ceramic sleeving. In addition, 0.625-inch-outside-diameter, 0.0125-inch-wall-thickness threaded stainless-steel tubes were installed in tapped holes in the thrust-chamber wrapping to serve as coolant static-pressure taps. A typical instrument array as described here is shown in figure 18.

Final Brazing and Heat Treating

A slurry of brazing material consisting of 82 percent nickel, 4.5 percent silicon, and 2.9 percent boron, with the balance iron and a trace of carbon suspended in acryloid cement and acetone was applied to appropriate portions of the instrumentation both outside and inside the thrust chamber. The chamber was then vacuum-brazed at about 1850° F to permanently attach the instruments.

The 1850° F brazing cycle also served as the solution-treatment of the type AM 350 stainless-steel wire wrap. At the completion of that cycle, the wrap was essentially in a fully annealed austenitic condition. To prevent later transformation of the wrap to the brittle martensitic form when contacted with liquid hydrogen, heat treatment was neces-

sary. The chamber was cold-soaked to -100° F for a minimum of 3 hours to transform the wrap to the martensitic phase. It was then heated to 1100° F for a minimum of 1 hour to produce a tempered martensitic form with restored ductility with high strength. This heat treating had no significant effect on the type 304 stainless-steel coolant channel material.

With moderate finishing, the inside chamber surface at the instrumentation stations was rendered reasonably smooth, with maximum projections of about 0.002 inch. If the subsequent pressure testing revealed leaks in the thrust chamber's outer wrapping, these were easily repairable with local low-temperature (about 460° F) solder application.

Final Fitting

To complete the fabrication procedure, the necessary fuel connectors were attached and the thermocouple leads were connected to terminal strips and connector plugs as described earlier. The coolant static-pressure taps were also connected to bracket-mounted fittings. Finally, to protect the instrumentation, the entire assembly was encased in a thin stainless-steel covering. This cover is visible in figure 19, which shows thrust chamber 1 completed and in position in the test facility, ready for operation.

APPENDIX B

SYMBOLS

A	cross-sectional or surface area, sq in.
$\overline{A}, \overline{D}, \overline{G}, \overline{\mu}, \overline{\rho}$	values averaged between stations n and n + 1
b	thickness, in.
c_p	specific heat at constant pressure, Btu/(lb)(^{o}R)
c*	characteristic exhaust velocity, ft/sec
D	hydraulic diameter, 4A/ wetted perimeter, in.
f	Fanning friction factor, dimensionless
G	weight-flow flux, w/A, lb/(sec)(sq in.)
g	gravitational conversion factor, 386.088 (lb_m/lb_f) (in./sec^2)
h	heat-transfer coefficient, Btu/(sq in.)(sec)(^{o}R) or lb/(sq in.)(sec)
i	enthalpy, Btu/lb
i*	reference enthalpy, Btu/lb
$\overline{K}$	heat-transfer correlation equation coefficient, dimensionless
k	thermal conductivity, Btu/(in.)(sec)(^{o}R)
L	channel inside width, in.
l	length, in.
Nu	Nusselt number, hD/k, dimensionless
Pr	Prandtl number, $c_p\mu/k$, dimensionless
p	stream static pressure, lb/sq in. abs
p_c	combustion chamber total pressure, lb/sq in. abs
Q	heat flow, Btu/sec
q	heat flux, Btu/(sec)(sq in.)
Re	Reynolds number, GD/μ, dimensionless
T	temperature, ^{o}R
w	weight-flow rate, lb/sec
δ	characteristic velocity pressure correction exponent, dimensionless
η_{c*}	characteristic velocity efficiency, percent
μ	viscosity, lb/(sec)(in.)
ρ	density, lb/cu in.

Subscripts:

A or I	thrust-chamber instrument station nearest injector
act	actual
aw	adiabatic wall
ch1	channel 1
ch2	channel 2

corr	corrected
F_2	fluorine
f	friction
g	gas or gas-side
H_2	hydrogen
i	enthalpy base
i*	reference enthalpy base
in	inlet to coolant manifold
Koo	Koo equation value
l	coolant or coolant-side
M	momentum
m	measured or midpoint
n, n+1	consecutive stations
s	stream static
T	total (pressure loss and coolant flow)
T_f	film temperature
T_s	static temperature
t	total
theo	theoretical
tht	nozzle throat
w	wall
1, 2, 3, 4, 5, 6, 7	thermocouple locations

Superscripts:

'	modified

REFERENCES

1. Douglass, H. W.; Hennings, G.; and Price, H. G., Jr.: Experimental Performance of Liquid Hydrogen and Liquid Fluorine in Regeneratively Cooled Rocket Engines. NASA TM X-87, 1959.

2. Curren, Arthur N.; Price, Harold G., Jr.; and Douglass, Howard W.: Analysis of Effects of Rocket-Engine Design Parameters on Regenerative-Cooling Capabilities of Several Propellants. NASA TN D-66, 1959.

3. Jones, William L.; Aukerman, Carl A.; and Gibb, John W.: Experimental Performance of a Hydrogen-Fluorine Rocket Engine at Several Chamber Pressures and Exhaust-Nozzle Expansion Area Ratios. NASA TM X-387, 1960.

4. Aukerman, Carl A.; and Church, Bruce E.: Experimental Hydrogen-Fluorine Rocket Performance at Low Pressures and High Area Ratios. NASA TM X-724, 1963.

5. Zeleznik, Frank J.; and Gordon, Sanford: A General IBM 704 or 7090 Computer Program for Computation of Chemical Equilibrium Compositions, Rocket Performance, and Chapman-Jouguet Detonations. NASA TN D-1454, 1962.

6. Gordon, Sanford; and Zeleznik, Frank J.: A General IBM 704 or 7090 Computer Program for Computation of Chemical Equilibrium Compositions, Rocket Performance, and Chapman-Jouget Detonations. Supplement I - Assigned Area-Ratio Performance. NASA TN D-1737, 1963.

7. Svehla, Roger A.: Thermodynamic and Transport Properties for the Hydrogen-Oxygen System. NASA SP-3011, 1964.

8. Harry, David P., III: Formulation and Digital Coding of Approximate Hydrogen Properties for Application to Heat-Transfer and Fluid-Flow Computations. NASA TN D-1664, 1963.

9. Price, Harold G., Jr.; Lubick, Robert J.; and Shinn, Arthur M., Jr.: Investigation of Injectors for a Low-Chamber-Pressure Hydrogen-Fluorine Rocket Engine. NASA TM X-485, 1962.

10. Jones, William L.; Price, Harold G., Jr.; and Lorenzo, Carl F.: Experimental Study of Zero-Flow Ejectors Using Gaseous Nitrogen. NASA TN D-203, 1960.

11. Krueger, Roger C.; and Curren, Arthur N.: Some factors Influencing Heat Transfer to Liquid-Propellant Rocket-Thrust-Chamber Coolant Channels. NASA TN D-3671, 1966.

12. Eckert, Ernst R. G.: Survey on Heat Transfer at High Speeds. (AF ARL-189), University of Minnesota, Dec. 1961.

13. Bartz, D. R.: A Simple Equation for Rapid Estimation of Rocket Nozzle Convective Heat Transfer Coefficients. Jet Propulsion, vol. 27, no. 1, Jan. 1957, pp. 49-51.

14. Schacht, Ralph, L.; Quentmeyer, Richard J.; and Jones, William L.: Experimental Investigation of Hot-Gas Side Heat-Transfer Rates for a Hydrogen-Oxygen Rocket. NASA TN D-2832, 1965.

15. Hendricks, R. C.; and Simon, F. F.: Heat Transfer to Hydrogen Flowing in a Curved Tube. Multi-Phase Flow Symposium. Norman J. Lipstein, ed., ASME, 1963, pp. 90-93.

16. Weiland, Walter F.: Measurement of Local Heat Transfer Coefficients for Flow of Hydrogen and Helium in a Smooth Tube at High Surface to Fluid Bulk Temperature Ratios. Paper presented at the Symposium on Nuclear Engineering Heat Transfer, AIChE, Chicago, Dec. 1962.

17. Hendricks, R. C.; Graham, R. W.; Hsu, Y. Y.; and Medeiros, A. A.: Correlation of Hydrogen Heat Transfer in Boiling and Supercritical Pressure States. ARS J., vol. 32, no. 2, Feb. 1962, pp. 244-252.

18. Miller, John V.; and Taylor, Maynard F.: Improved Method of Predicting Surface Temperatures in Hydrogen-Cooled Nuclear Rocket Reactor at High Surface-to Bulk-Temperature Ratios. NASA TN D-2594, 1965.

19. McAdams, William H.: Heat Transmission. Third ed., McGraw-Hill Book Co., Inc., 1954.

TABLE I. - THRUST CHAMBER COOLANT CHANNEL DIMENSIONS

[Coolant flow path distance from nozzle exit location to station XV for chamber 2, 3.445 in.; coolant flow path distance from station I to injector location, 1.967 in. Channel 1 of each chamber contains coolant static-pressure taps.]

Chamber inside diameter,[a] in.	Location	Chamber area ratio,[a] A/A_{tht}	Channel bottom inside arc width,[a] in.	Thrust chamber 1; station spacing, 1.5 in.						Thrust chamber 2; station spacing, 1.0 in.					
				Station	Average channel height,[b] in.	Channel 1 height,[b] in.	Channel 1 flow area,[c] A_l, $in.^2$	Channel 2 height,[b] in.	Channel 2 flow area,[c] A_l, $in.^2$	Station	Average channel height,[b] in.	Channel 1 height,[b] in.	Channel 1 flow area,[c] A_l, $in.^2$	Channel 2 height,[b] in.	Channel 2 flow area,[c] A_l, $in.^2$
5.386	Injector	1.897	0.190												
5.386										I	0.069	0.067	0.013	0.072	0.014
5.386										II	.070	.068	.013	.074	.014
5.386										III	.071	.069	.013	.075	.015
5.386				A	0.070	0.068	0.013	0.072	0.014						
5.386										IV	.071	.070	.014	.075	.015
5.379		1.893		B	.068	.066	.013	.069	.013	V	.065	.064	.012	.070	.014
5.305		1.841	.186							VI	.069	.068	.013	.071	.014
5.234		1.792	.183	C	.073	.069	.013	.073	.014						
5.146		1.732	.180							VII	.072	.070	.013	.075	.014
4.902		1.572	.169	D	.073	.068	.012	.069	.012	VIII	.068	.066	.011	.070	.012
4.574		1.368	.155							IX	.064	.064	.010	.066	.011
4.375		1.252	.146	E	.065	.063	.009	.065	.010						
4.162		1.133	.137							X	.058	.056	.008	.061	.009
3.910	Throat	1.000	.126	F	.061	.059	.008	.063	.008	XI	.062	.060	.008	.060	.008
4.164		1.134	.137							XII	.077	.074	.010	.076	.011
4.243		1.178	.140	G	.080	.079	.012	.082	.013						
4.681		1.433	.159							XIII	.092	.089	.015	.090	.015
5.199		1.768	.182	H	.104	.104	.019	.106	.020	XIV	.104	.103	.019	.105	.020
5.717		2.138	.204							XV	.112	.111	.023	.114	.024
7.500	Nozzle exit	3.679	.282												

[a] Design value.

[b] Measured value.

[c] Calculated value.

TABLE II. - SOME PROPERTIES OF PRODUCTS OF COMBUSTION OF

(a) Specific heat, viscosity, thermal

Pressure, p, $\frac{lb}{sq\ in.}$ abs	Temperature, T, ^oR	Specific heat at constant pressure, c_p, $\frac{Btu}{(lb)(^oR)}$	Viscosity, μ, $\frac{lb}{(sec)(in.)}$	Thermal conductivity, k, $\frac{Btu}{(in.)(sec)(^oR)}$	Enthalpy, i, $\frac{Btu}{lb}$
		12 Percent hydrogen by weight			
60	540	0.5731	0.7563×10^{-6}	1.019×10^{-6}	-5400
	1000	.5782	1.388	1.682	-5135
	1500	.5864	2.027	2.367	-4845
	2000	.6056	2.619	3.079	-4547
	2500	.6298	3.167	3.808	-4238
	3000	.6533	3.676	4.557	-3917
	3500	.6819	4.155	5.438	-3584
	4000	.7393	4.609	6.963	-3231
	4500	.8671	5.044	10.15	-2833
	5000	1.118	5.462	16.58	-2343
	5263.2	1.316	5.675	21.82	-2024
	5500	1.539	5.862	27.78	-1687
	5709.6	1.773	6.022	34.02	-1341
	6000	2.149	6.237	43.87	-772
	6193.8	2.429	6.373	50.93	-328
37.3	540	0.5735	0.7564×10^{-6}	1.019×10^{-6}	-5400
	1000	.5783	1.388	1.682	-5135
	1500	.5859	2.027	2.367	-4845
	2000	.6055	2.619	3.079	-4547
	2500	.6303	3.167	3.803	-4238
	3000	.6539	3.676	4.568	-3917
	3500	.6845	4.155	5.488	-3584
	4000	.7527	4.609	7.234	-3226
	4500	.9109	5.044	11.07	-2815
	5000	1.224	5.462	18.95	-2290
	5500	1.744	5.858	32.53	-1558
	6000	2.480	6.224	51.22	-508
14.7	540	0.5728	0.7564×10^{-6}	1.019×10^{-6}	-5400
	1000	.5784	1.388	1.682	-5135
	1500	.5859	2.027	2.367	-4845
	2000	.6061	2.619	3.079	-4547
	2500	.6301	3.167	3.785	-4238
	3000	.6539	3.677	4.595	-3917
	3500	.6937	4.155	5.626	-3581
	4000	.7936	4.609	7.997	-3214
	4500	1.032	5.042	13.63	-2765
	5000	1.512	5.454	25.39	-2141
	5500	2.296	5.841	44.80	-1201
	6000	3.305	6.186	67.84	194

[a]Most values interpolated.

HYDROGEN-FLUORINE PROPELLANT COMBINATION, ASSUMING EQUILIBRIUM COMPOSITION[a]

conductivity, and enthalpy variation with temperature and pressure

Specific heat at constant pressure, c_p, Btu/(lb)(^oR)	Viscosity, μ, lb/(sec)(in.)	Thermal conductivity, k, Btu/(in.)(sec)(^oR)	Enthalpy, i, Btu/lb	Specific heat at constant pressure, c_p, Btu/(lb)(^oR)	Viscosity, μ, lb/(sec)(in.)	Thermal conductivity, k, Btu/(in.)(sec)(^oR)	Enthalpy, i, Btu/lb
15 Percent hydrogen by weight				18 Percent hydrogen by weight			
0.6698	0.7610×10^{-6}	1.232×10^{-6}	-5216	0.7668	0.7574×10^{-6}	1.405×10^{-6}	-5031
.6770	1.362	1.984	-4906	.7758	1.330	2.226	-4676
.6866	1.959	2.751	-4565	.7866	1.889	3.063	-4286
.7088	2.504	3.547	-4217	.8121	2.395	3.925	-3887
.7370	3.007	4.369	-3855	.8445	2.859	4.815	-3473
.7649	3.473	5.203	-3480	.8765	3.290	5.723	-3043
.8000	3.912	6.197	-3090	.9179	3.696	6.810	-2595
.8725	4.330	7.952	-2674	1.005	4.084	8.748	-2117
1.036	4.731	11.66	-2202	1.203	4.460	12.87	-1571
1.358	5.120	19.19	-1612	1.596	4.826	21.26	-881
1.615	5.320	25.35	-1222	1.909	5.014	28.15	-422
1.904	5.496	32.39	-806	------	----------	----------	-----
2.208	5.647	39.80	-376	------	----------	----------	-----
------	----------	----------	-----	------	----------	----------	-----
------	----------	----------	-----	------	----------	----------	-----
0.6697	0.7611×10^{-6}	1.232×10^{-6}	-5216	0.7665	0.7576×10^{-6}	1.405×10^{-6}	-5031
.6772	1.362	1.984	-4906	.7760	1.330	2.226	-4676
.6865	1.959	2.751	-4565	.7867	1.889	3.063	-4286
.7086	2.504	3.547	-4217	.8119	2.395	3.925	-3887
.7371	3.007	4.362	-3855	.8445	2.859	4.812	-3472
.7656	3.473	5.212	-3480	.8773	3.289	5.734	-3042
.8040	3.912	6.255	-3089	.9229	3.695	6.875	-2594
.8902	4.329	8.266	-2668	1.027	4.082	9.099	-2110
1.092	4.731	12.74	-2179	1.272	4.458	14.07	-1543
1.495	5.119	21.96	-1542	1.763	4.824	24.37	-796
2.174	5.491	38.04	-637	------	----------	----------	-----
------	----------	----------	-----	------	----------	----------	-----
0.6694	0.7613×10^{-6}	1.232×10^{-6}	-5216	0.7662	0.7576×10^{-6}	1.405×10^{-6}	-5032
.6774	1.362	1.984	-4905	.7764	1.330	2.226	-4676
.6857	1.958	2.751	-4566	.7856	1.889	3.063	-4286
.7095	2.504	3.547	-4217	.8128	2.395	3.925	-3887
.7378	3.007	4.338	-3855	.8454	2.859	4.780	-3472
.7657	3.473	5.249	-3480	.8777	3.289	5.774	-3042
.8150	3.911	6.414	-3086	.9362	3.695	7.052	-2590
.9428	4.327	9.159	-2651	1.091	4.083	10.10	-2090
1.250	4.728	15.74	-2114	1.465	4.458	17.43	-1464
1.872	5.114	29.57	-1349	2.226	4.821	32.88	-560
2.902	5.476	52.76	-172	------	----------	----------	-----
------	----------	----------	-----	------	----------	----------	-----

TABLE II. - Concluded. SOME PROPERTIES OF PRODUCTS OF COMBUSTION OF HYDROGEN-FLUORINE PROPELLANT COMBINATION, ASSUMING EQUILIBRIUM COMPOSITION[a]

(b) Static temperature and pressure variation with area ratio

Area ratio, $\frac{A}{A_{tht}}$	Temperature, T, ^{o}R	Pressure, p, $\frac{lb}{sq\ in.}$ abs	Temperature, T, ^{o}R	Pressure, p, $\frac{lb}{sq\ in.}$ abs	Temperature, T, ^{o}R	Pressure, p, $\frac{lb}{sq\ in.}$ abs
	12 Percent hydrogen by weight		15 Percent hydrogen by weight		18 Percent hydrogen by weight	
1.897	6193.8	60.00	5709.6	60.00	5263.2	60.00
1.5	6075	53.25	5620	53.23	5150	53.20
1.0	5803.2	34.21	5308.2	34.05	4822.2	33.70
1.5	5160	13.20	4610	12.60	3940	12.00
2.0	4835	7.85	4210	7.70	3515	6.80
2.5	4585	5.20	3935	4.70	3235	4.35
3.0	4380	3.75	3710	3.35	3030	3.00
3.5	4240	3.10	3520	2.95	2850	2.45
4.0	4080	2.75	3355	2.55	2690	2.05
4.5	3960	2.35	3215	2.10	2560	1.95

(c) Pressure correction for c*

$c^*_{corr} = c^*(p_c/60)^{\delta}$		
Percent hydrogen	Characteristic exhaust velocity, c*, ft/sec	δ
12	8162	0.01239
15	8314	.00913
18	8393	.00512

[a]Most values interpolated.

TABLE III. - SUMMARY OF EXPERIMENTAL RUN CONDITIONS

Run	Thrust chamber	Injector elements	Combustion pressure, p_c, $\frac{lb}{sq\ in.}$ abs	Hydrogen by weight in hydrogen-fluorine, percent	Total chamber hydrogen flow rate, $w_{H_2, T}$, $\frac{lb}{sec}$	Fluorine flow rate, w_{F_2}, $\frac{lb}{sec}$	Hydrogen injector pressure drop, $\frac{lb}{sq\ in.}$	Fluorine injector pressure drop, $\frac{lb}{sq\ in.}$	Characteristic velocity efficiency, η_c, percent
1	1	121	59.45	12.01	0.3436	2.517	15.88	33.44	98.83
2	1	121	58.74	12.09	.3458	2.514	15.47	59.00	97.36
3	1	121	60.77	12.14	.3446	2.495	13.80	30.34	100.94
4	1	131	59.46	12.32	.3425	2.437	12.77	-----	100.79
5	1	121	58.00	15.12	.4242	2.382	17.71	58.14	98.19
6	1	121	60.60	15.15	.4241	2.375	16.41	29.01	100.30
7	1	131	59.48	15.43	.4232	2.319	12.14	-----	100.33
8	1	131	49.22	15.04	.3443	1.945	10.06	-----	99.81
9	2	121	59.83	18.03	.5026	2.285	15.32	35.00	98.76
10	2	131	60.22	18.10	.5046	2.284	16.98	56.86	99.44

TABLE IV. - SUMMARY OF EXPERIMENTAL DATA USED IN PLOTS

(a) Coolant and midwall temperatures for thrust chamber 1

Run	Reading	Channel	Instrument stations									
			Coolant outlet	A	B	C	D	E	F	G	H	Coolant inlet
			Temperature, T, ^{o}R									
1	T_3	1	(a)	549.81	490.32	436.11				195.25		(a)
		2	(a)		465.34	378.39		380.98	332.39	148.20	170.26	(a)
	T_4	1	--	1528.4	1967.7	1668.1	1741.0	1707.4		1084.2	1351.3	--
2	T_3	1	(a)	646.92	586.53	352.22		396.31		205.23		(a)
		2	(a)		397.22	318.45		321.88		138.03	158.53	(a)
	T_4	1	--	1591.2	2178.5	1860.4	1890.1	1864.8		1206.1	1498.5	--
3	T_3	1	(a)	526.55	479.46	436.22				165.11		(a)
		2	(a)		334.54	276.55		271.07		124.62	129.50	(a)
	T_4	1	--	1415.8	2001.0	1640.2	1663.6	1684.2		1045.4	1334.2	--
4	T_3	1	(a)	628.72	572.92	513.52				205.96		(a)
		2	(a)		491.33	397.85		392.42		160.76	187.16	(a)
	T_4	1	--	1649.8	2235.6	1848.8	1873.6	1845.4		1185.2	1475.2	--
5	T_3	1	(a)	383.95	345.60	317.65				133.34		(a)
		2	(a)		320.17	247.27		248.81		109.38	129.27	(a)
	T_4	1	--	1110.6	1448.1	1236.7	1282.6	1325.8		762.28	1039.1	--
6	T_3	1	(a)	435.16	396.58	362.94				130.64		(a)
		2	(a)		264.99	232.62		224.55		104.84	122.69	(a)
	T_4	1	--	1284.4	1751.4	1452.1	1513.1	1556.7		921.30	1213.3	--
7	T_3	1	(a)	354.06	315.64	292.92				125.60		(a)
		2	(a)		349.95	290.40		282.95		109.18	149.22	(a)
	T_4	1	--	879.29	1362.0	1158.6	1224.8	1282.4		745.36	1030.0	--
8	T_3	1	(a)	336.20	305.62	283.75				121.89		(a)
		2	(a)		367.57	298.53		396.54		113.52	162.34	(a)
	T_4	1	--	803.68	1223.7	1040.6	1084.0	1132.7		672.31	944.16	--

[a]Refer to coolant manifold temperature tabulations.

TABLE IV. - Continued. SUMMARY OF EXPERIMENTAL DATA USED IN PLOTS

(b) Coolant and midwall temperatures for thrust chamber 2

Run	Reading	Channel	Instrument stations															
			Coolant outlet	I	II	III	IV	V	VI	VII	VIII	IX	X	XI	XII	XIII	XIV	XV	Coolant inlet
			Temperature, T, ^{o}R																
9	T_3	1	(a)		336.51	298.91	272.90	246.66	230.52	203.87				161.55	89.23	101.24	67.77		(a)
		2	(a)	301.94		261.73	241.58	221.66	193.59	171.98	179.51	158.45	115.80	109.30	97.14		63.40	80.45	(a)
	T_4	1	--	837.53	822.57	985.66	1056.7	1052.4	1156.2		1063.0	1137.2	985.34		618.15	962.76			--
		2	--	825.36	1045.1		1146.1	1102.9	1224.3	1175.9	1046.2		1057.9	860.73	792.69		980.56	837.40	--
10	T_3	1	(a)		339.67			275.33	249.30	226.82	192.31	152.75	134.49	190.72	85.79	107.57			(a)
		2	(a)	320.00			259.00		209.19	181.49	197.71	161.25	122.15	107.63	98.01		79.63	91.31	(a)
	T_4	1	--	936.19		1047.6	1248.3	1245.5	1335.3		1200.1	1285.0			700.36	1059.6			--
		2	--		1084.0				1262.4			1106.3	1099.4	816.53	843.48			1045.3	--

(c) Coolant static pressures (channel 1)

Run	Instrument stations																		
	Coolant outlet	I	II	III	A	IV	B, V	VI	C	VII	D, VIII	IX	E	X	F, XI	XII	G	XIII	H, XIV	XV	Coolant inlet
	Pressure, p, lb/sq. in. abs																				
1	75.84	-----	--	-----	98.61	--	102.00	--	106.95	------	110.86	------	111.67	--	116.02	--	124.53	------	127.07	------	127.98
2	75.14	-----	--	-----	96.64	--	99.78	--	101.62	------	105.28	------	107.45	--	110.64	--	120.21	------	122.68	------	123.63
3	76.65	-----	--	-----	98.06	--	101.43	--	103.46	------	107.20	------	109.48	--	112.94	--	123.41	------	125.89	------	126.73
4	74.32	-----	--	-----	100.66	--	104.19	--	109.42	------	113.12	------	114.04	--	118.12	--	126.51	------	129.07	------	130.05
5	76.01	-----	--	-----	99.05	--	102.29	--	104.34	------	108.40	------	110.79	--	114.55	--	125.90	------	128.57	------	129.58
6	78.48	-----	--	-----	102.78	--	106.46	--	108.91	------	113.06	------	115.59	--	119.41	--	131.11	------	133.75	------	134.63
7	73.94	-----	--	-----	97.43	--	100.84	--	106.56	------	110.82	------	112.01	--	117.11	--	126.59	------	129.16	------	130.02
8	61.88	-----	--	-----	81.45	--	84.31	--	89.07	------	92.57	------	93.63	--	97.86	--	105.80	------	107.93	------	108.69
9	77.57	81.32	--	93.19	------	--	100.47	--	------	107.04	------	110.03	------	--	120.02	--	------	131.39	------	132.70	133.15
10	81.44	-----	--	99.89	------	--	108.87	--	------	116.65	------	120.04	------	--	130.03	--	------	143.33	------	144.74	145.24

[a]Refer to coolant manifold temperature tabulations.

TABLE IV. - Concluded. SUMMARY OF EXPERIMENTAL DATA USED IN PLOTS

(d) Coolant manifold temperatures

Run	Coolant outlet manifold (thermocouples)				Coolant inlet manifold (carbon resistors)	
	1	2	3	4	1	2
	Temperature, T, ^{o}R					
1	516.06	494.01	649.18	552.34	54.85	54.88
2	466.47	521.10	631.43	791.25	54.33	54.36
3	368.80	463.97	654.57	675.33	53.73	54.53
4	483.05	695.35	568.95	690.98	55.68	55.14
5	366.49	420.11	500.08	508.58	54.85	54.88
6	320.86	393.39	613.95	580.56	55.13	54.88
7	383.68	487.29	392.22	463.29	55.68	55.15
8	392.32	511.55	386.03	436.16	53.69	53.22
9	325.81		290.70	328.12	53.48	54.74
10	341.55	356.45	326.94	338.81	54.10	55.93

TABLE V. - SUMMARY OF EXPERIMENTAL DATA NOT USED IN PLOTS

[Channel 1 has coolant static-pressure taps.]

(a) Outer wire wrap and midwall temperatures for thrust chamber 1

Run	Reading	Channel	Instrument stations							
			A	B	C	D	E	F	G	H
			Temperature, T, ^{o}R							
1	T_2	1	1807.5	1894.5		1119.0	859.20	784.15	1176.7	
		2	1237.2	1656.3	1682.4	1546.4	1435.3	1187.9	915.87	
	T_5	1		505.20		407.60			238.09	227.69
		2	549.44	464.83	407.33			317.49	277.07	
	T_4	2		1654.2			1598.6			
2	T_2	1								
		2			1365.3	1295.9	1262.9	1033.8	782.02	
	T_5	1		595.30	538.95			383.58	272.41	260.27
		2	551.50	398.43	421.42			269.88	217.49	219.50
	T_4	2		1325.7			1399.3			
3	T_2	1		1988.8		1113.0	881.23	741.58	1151.7	
		2	787.00		1180.6	1138.5	1157.8	930.24	717.04	
	T_5	1		490.62				320.04		222.46
		2	377.48	337.57	288.03	243.67		218.07	149.79	144.66
	T_4	2		1195.3			1281.9			
4	T_2	1		2097.2		1234.1		844.22	1272.8	
		2	1146.1		1686.1	1625.7	1567.9	1262.2	919.67	
	T_5	1		589.78				380.38		
		2	580.62	503.02	447.81	317.32		323.30	312.82	309.70
	T_4	2		1727.0			1630.2			

TABLE V. - Continued. SUMMARY OF EXPERIMENTAL DATA NOT USED IN PLOTS

[Channel 1 has coolant static-pressure taps.]

(a) Concluded. Outer wire wrap and midwall temperatures for thrust chamber 1

Run	Reading	Channel	Instrument stations							
			A	B	C	D	E	F	G	H
			Temperature, T, ^{o}R							
5	T_2	1								
		2			1091.4	1032.7	1073.4	856.37	645.41	
	T_5	1		357.62	328.06			237.92	185.17	169.27
		2		295.34				224.66	150.00	139.78
	T_4	2		1070.0			1188.0			
6	T_2	1		1717.9		970.98	728.08	660.93	1026.4	
		2	602.95		945.17	922.26	1005.1	795.66	605.10	
	T_5	1		396.69				265.31		184.04
		2	293.18	247.49	231.00	219.17		176.65	146.83	133.74
	T_4	2		985.94			1134.5			
7	T_2	1		1266.1		785.41		570.78	837.40	
		2	725.29		1288.6	1213.4	1183.4	979.25	739.55	
	T_5	1		326.65				218.20		160.16
		2	392.10	355.87	312.33	269.07		242.71		
	T_4	2		1252.9			1286.1			
8	T_2	1		1156.4		718.31		506.76	750.00	
		2	741.56		1293.2	1224.9	1144.1	918.38	699.78	
	T_5	1		311.03				210.20		147.90
		2	411.94	375.04	336.38	278.02		247.02		
	T_4	2		1237.9			1252.9			

TABLE V. - Concluded. SUMMARY OF EXPERIMENTAL DATA NOT USED IN PLOTS

[Channel 1 has coolant static-pressure taps.]

(b) Outer wire wrap and midwall temperatures for thrust chamber 2

Run	Thermo-couple	Channel	Instrument stations														
			I	II	III	IV	V	VI	VII	VIII	IX	X	XI	XII	XIII	XIV	XV
			Temperature, T, ^{o}R														
9	T_2	1	813.64	835.65	923.46	934.19			876.30	1006.7	1056.3	805.18		692.66	951.60	825.64	760.91
		2	751.39	951.69	1055.1		1042.9	1107.9		1057.3	948.71	898.98	751.12	828.77	902.90	962.5	834.45
	T_5	1		346.35	318.71	308.22	291.21	269.62	238.28	213.47	190.25	194.63	143.30	115.94	113.91	109.76	115.29
		2		307.66		265.33	243.98	227.60	192.80	173.78		199.47	140.89	124.05	128.39	103.36	122.93
10	T_2	1	947.23		999.64				966.02	1097.5	1167.1	902.78		553.75	1054.3	482.26	812.56
		2			1074.1		1091.6			1054.5	961.88	940.53	588.13	858.85	950.95	1035.5	1018.2
	T_5	1	395.51	389.22	348.53	331.58	313.29	288.13	253.36	225.48	202.43	207.42	156.23	108.96		116.67	
		2		315.40	294.98		251.58	234.05	199.16	177.55			160.42	126.30	121.92		

TABLE VI. - COOLANT CHANNEL WEIGHT FLOW RATE DISTRIBUTION SUMMARY

Run	Thrust chamber	Channel	Individual channel hydrogen weight-flow rate, w_{H_2}, lb/sec	Percent of average (for 72 channels) hydrogen weight-flow rate	Run	Thrust chamber	Channel	Individual channel hydrogen weight-flow rate, w_{H_2}, lb/sec	Percent of average (for 72 channels) hydrogen weight-flow rate
1	1	1	46×10^{-4}	96.4	6	1	1	46.20×10^{-4}	78.4
		2	49.44×10^{-4}	103.6			2	71.61×10^{-4}	121.6
2	1	1	38.03×10^{-4}	79.2	[a]7	1	1	61.91×10^{-4}	105.3
		2	52.08×10^{-4}	120.8			2	55.65×10^{-4}	94.7
3	1	1	39.77×10^{-4}	83.1	[a]8	1	1	53.48×10^{-4}	111.8
		2	55.95×10^{-4}	116.9			2	42.17×10^{-4}	88.2
4	1	1	43.52×10^{-4}	91.5	9	2	1	63.91×10^{-4}	91.6
		2	51.62×10^{-4}	108.5			2	75.70×10^{-4}	108.4
5	1	1	56.24×10^{-4}	95.5	10	2	1	64.49×10^{-4}	92.0
		2	61.60×10^{-4}	104.5			2	75.68×10^{-4}	108.0

[a]Runs 7 and 8 show a reversal in channels' relative weight-flow rates compared to runs 1 to 6. This was due to minor thrust-chamber repairs following run 6 which apparently affected relative channel blockage.

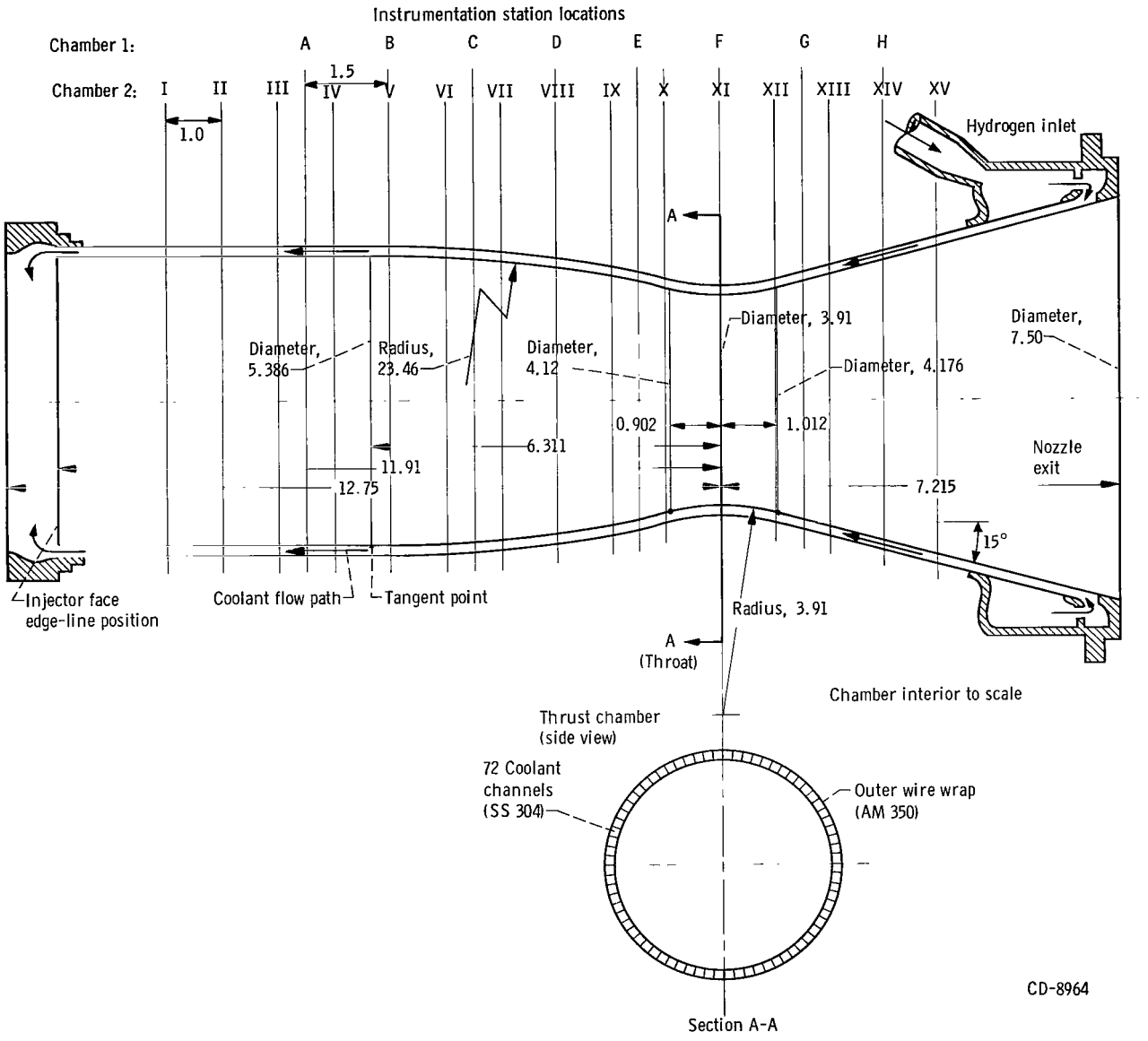

Figure 1. - Thrust-chamber configuration details and instrumentation station locations. (All dimensions in inches unless otherwise noted.)

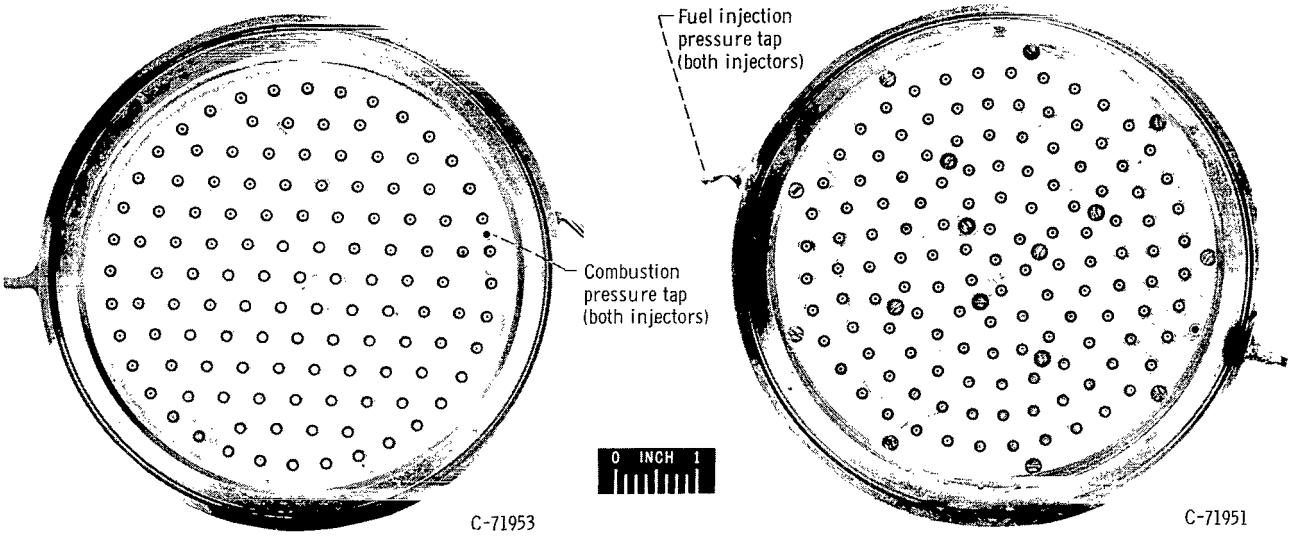

(a) Face view of 121-coaxial-element, dished-face, hexagonal-pattern injector.

(b) Face view of 131-coaxial-element, flat-face, ring-pattern injector.

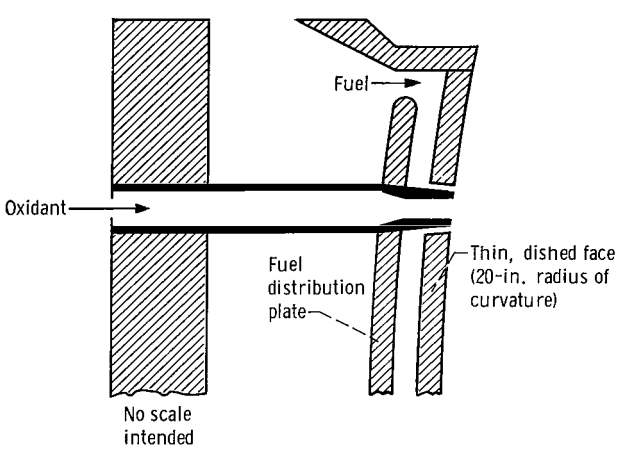

(c) Section view of 121-element injector.

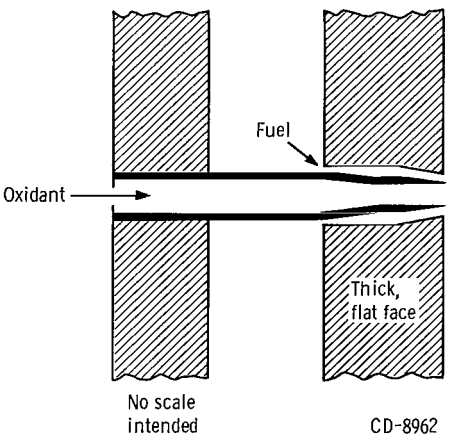

(d) Section view of 131 element injector.

Number of elements	121	131
Face material	Nickel	Copper
Face thickness, in.	0.084	0.700
Total hydrogen orifice area, sq in.	1.2054	1.1750
Total fluorine orifice area, sq in.	0.08131	0.0643
Fluorine orifice convergence angle, deg	15	10

Figure 2. - Injector configuration details.

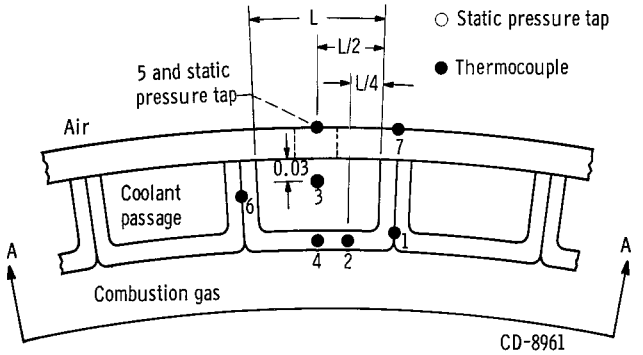

(a) Coolant channel section showing composite station instrumentation.

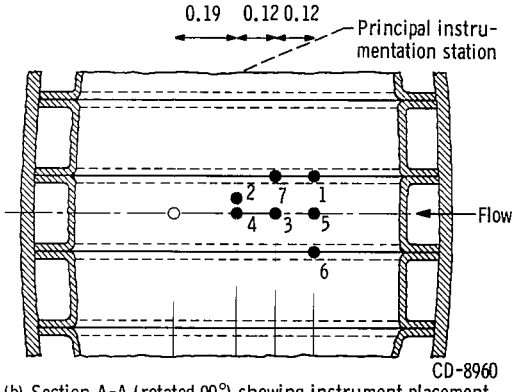

(b) Section A-A (rotated 90°) showing instrument placement in channel 1 of thrust chamber 1.

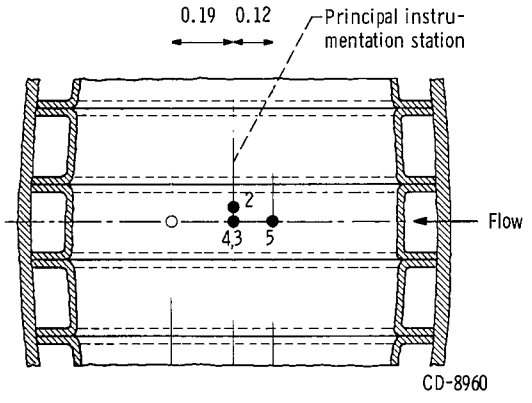

(c) Section A-A (rotated 90°) showing instrument placement in channel 1 of thrust chamber 2.

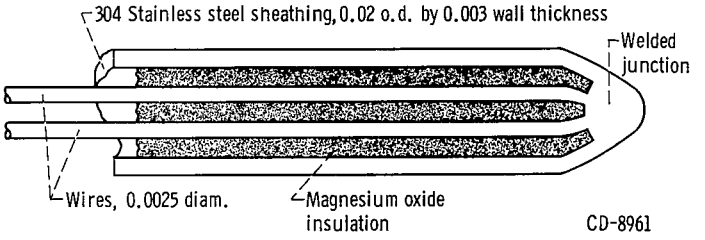

(d) Thermocouple detail. Two types: Chromel-Alumel (thermocouples 1, 2, and 4) and copper constantan (thermocouples 3, 5, 6, and 7). Static pressure tap is 0.0625 inch o.d. by 0.0125 inch wall thickness stainless steel tubing.

Figure 3. - Instrument array details for rocket engine thrust-chamber coolant passages and walls. Geometry scaled approximately to stations H or XIV of chambers 1 and 2, respectively. (All dimensions in inches.)

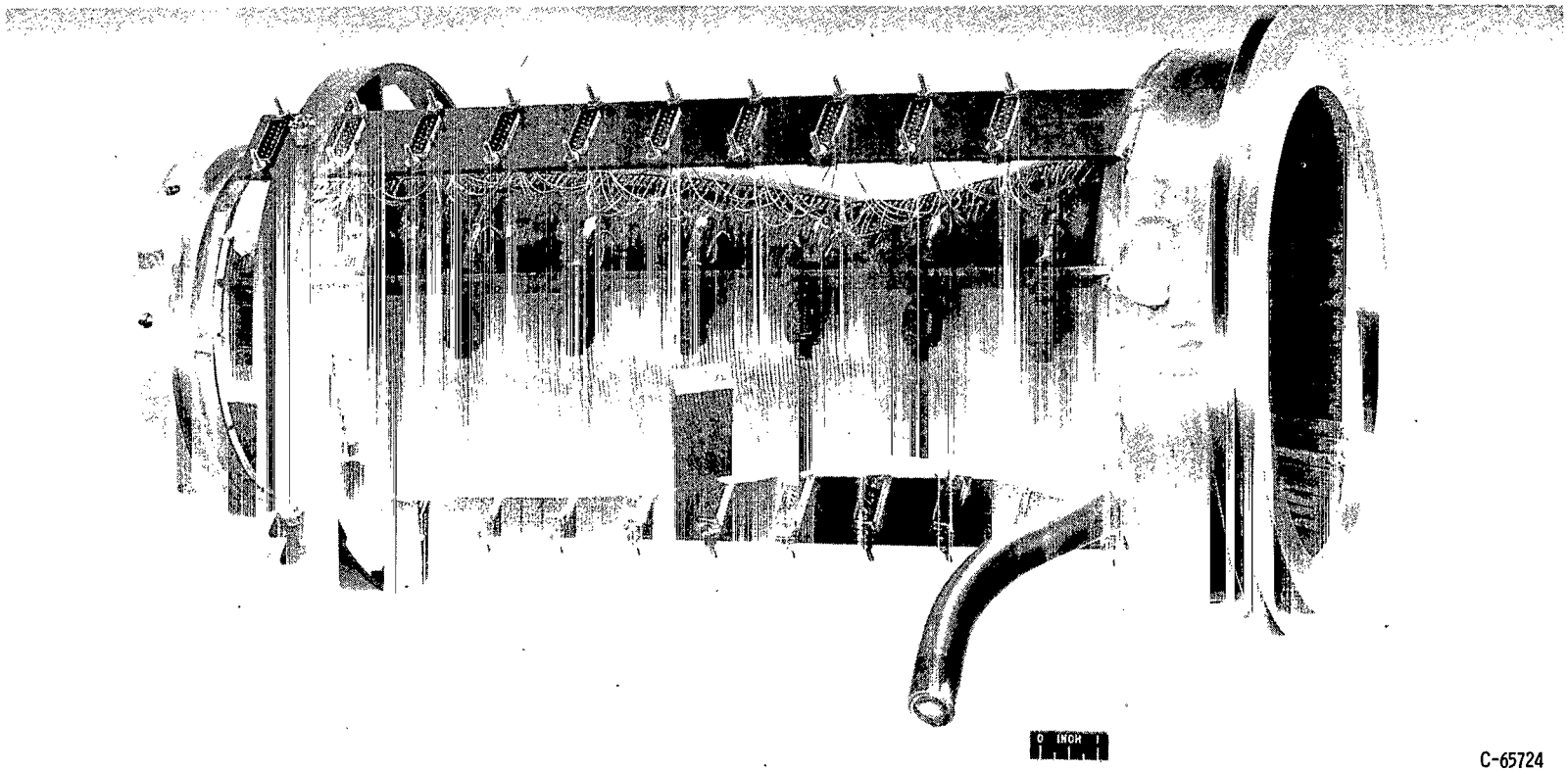

C-65724

Figure 4. - Thrust chamber 2 immediately prior to attachment of protective cover and fuel inlet fitting.

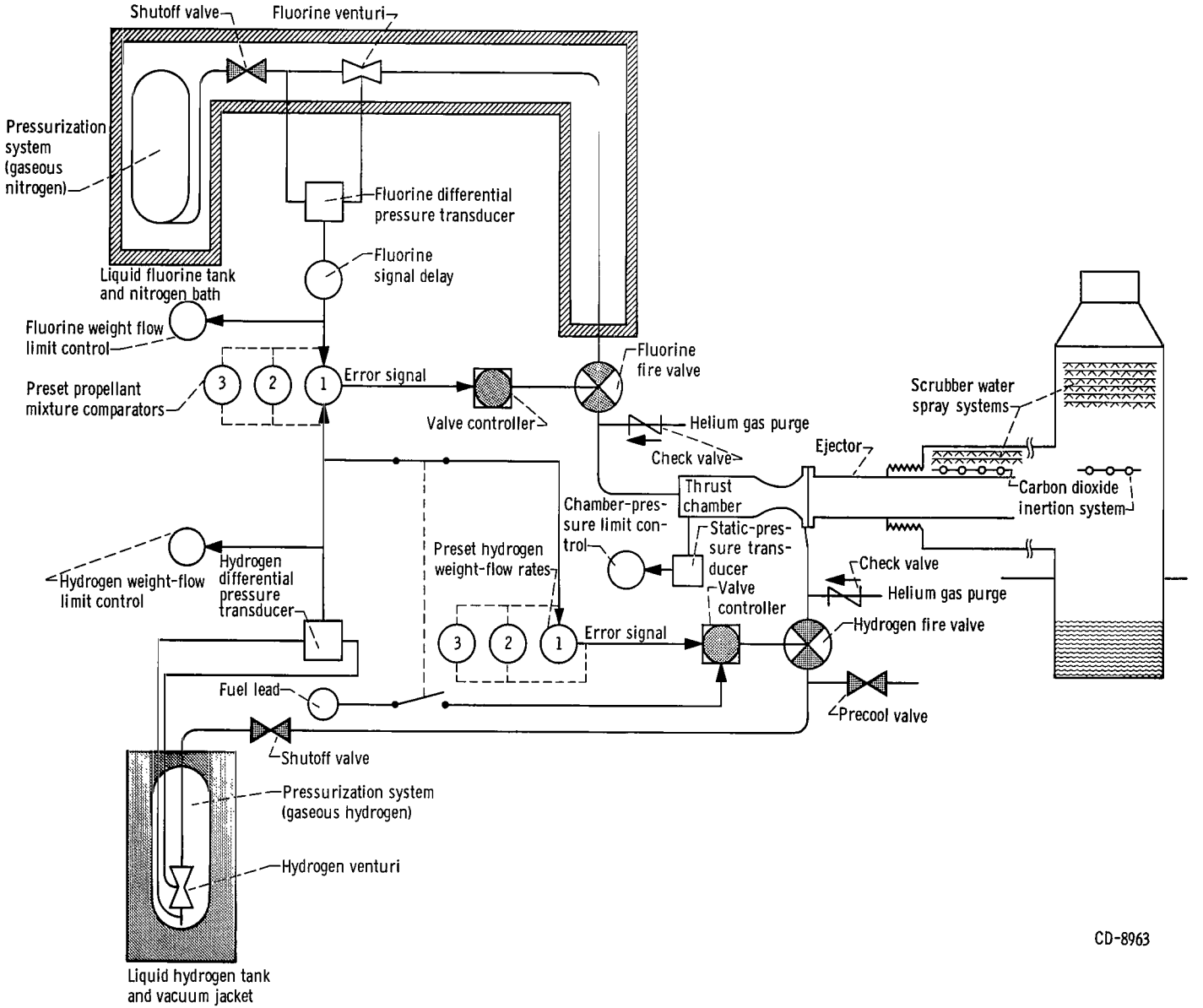

Figure 5. - Thrust-chamber installation and metering and control system.

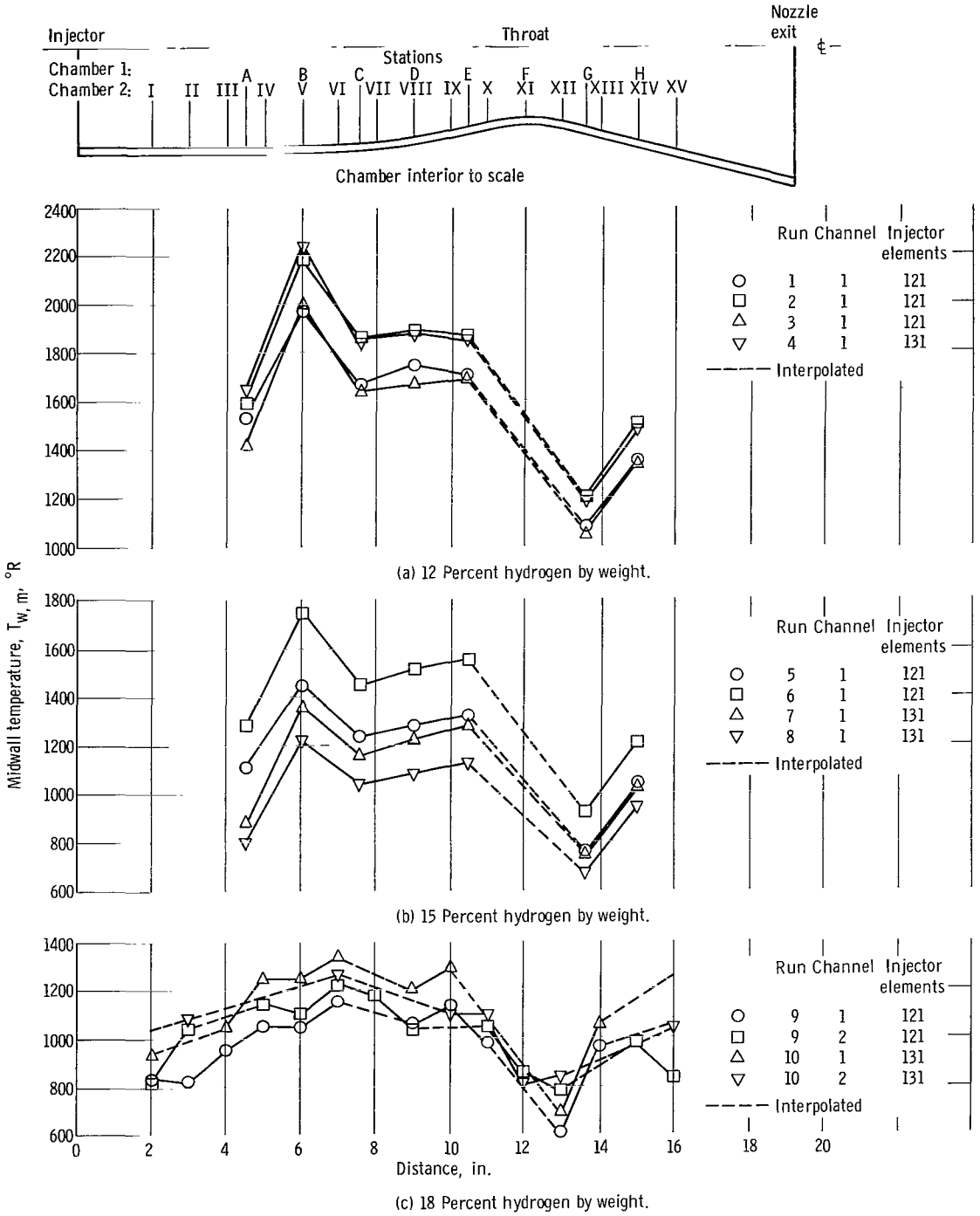

Figure 6. - Hydrogen-fluorine rocket engine thrust-chamber midwall temperature profiles obtained at 60-pounds-per-square-inch-absolute (50-lb/sq in. abs for run 8) combustion pressure.

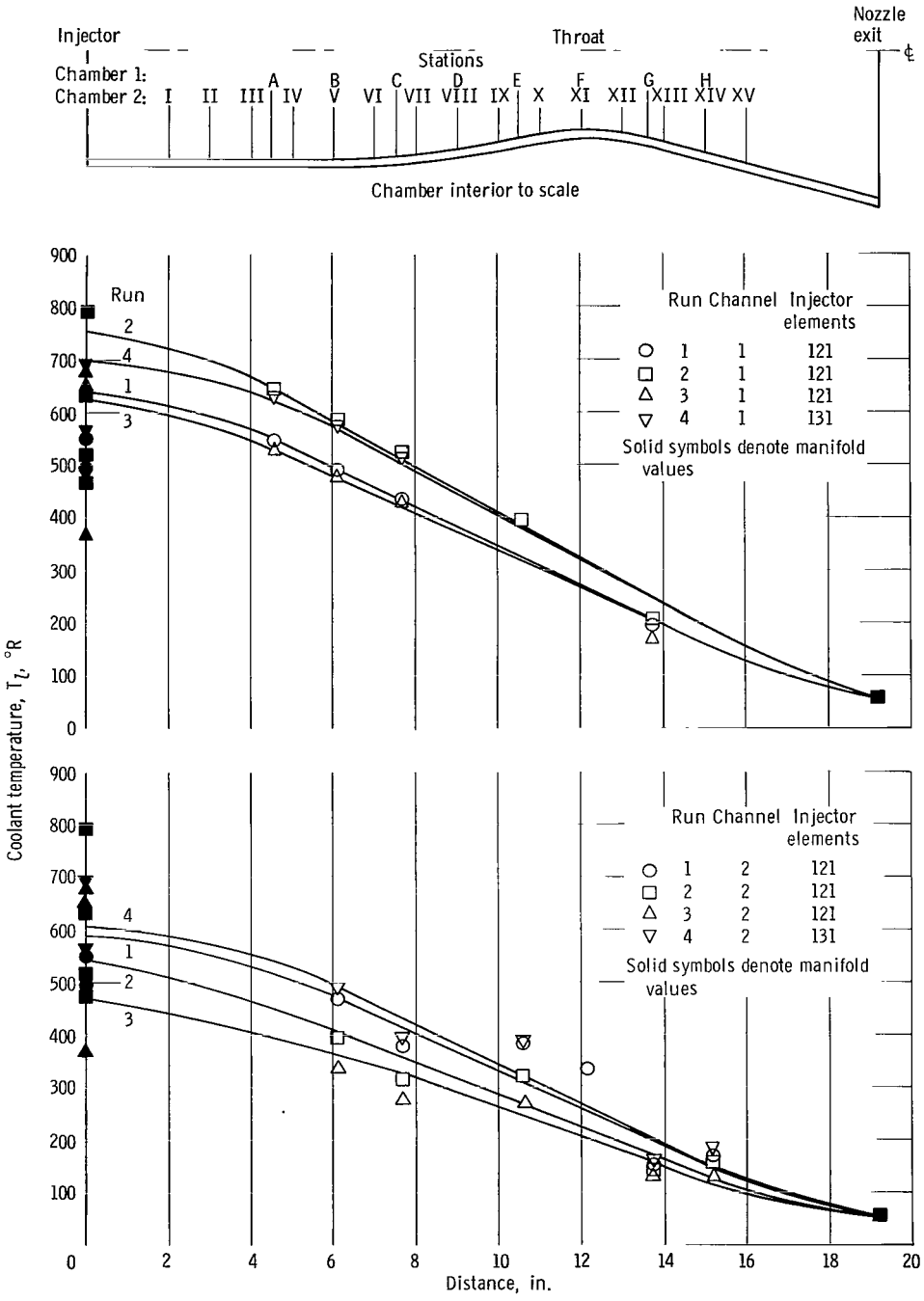

(a) 12 Percent hydrogen by weight.

Figure 7. - Hydrogen-fluorine rocket engine thrust-chamber coolant temperature profiles obtained at 60-pounds-per-square-inch-absolute (50-lb/sq in. abs for run 8) combustion pressure.

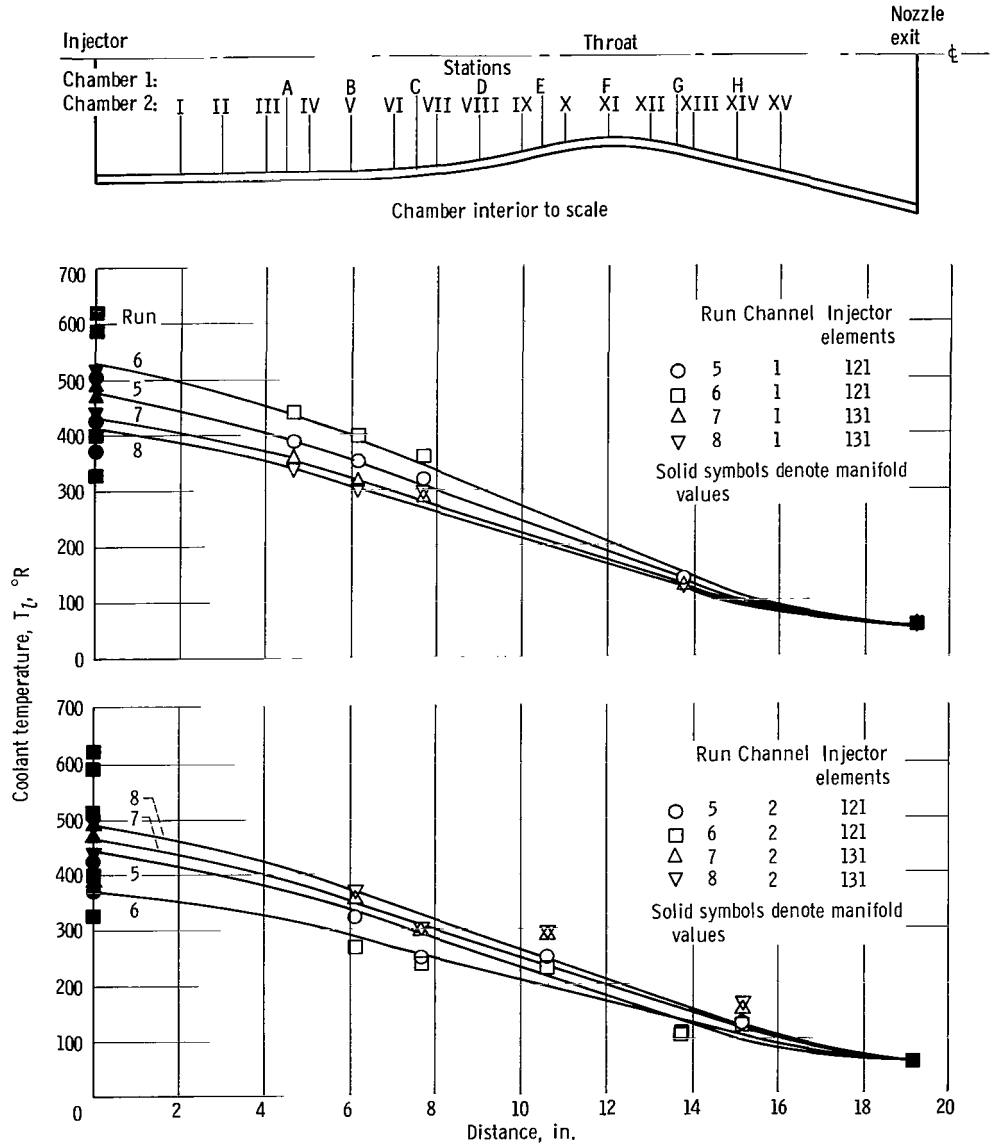

(b) 15 Percent hydrogen by weight.

Figure 7. - Continued.

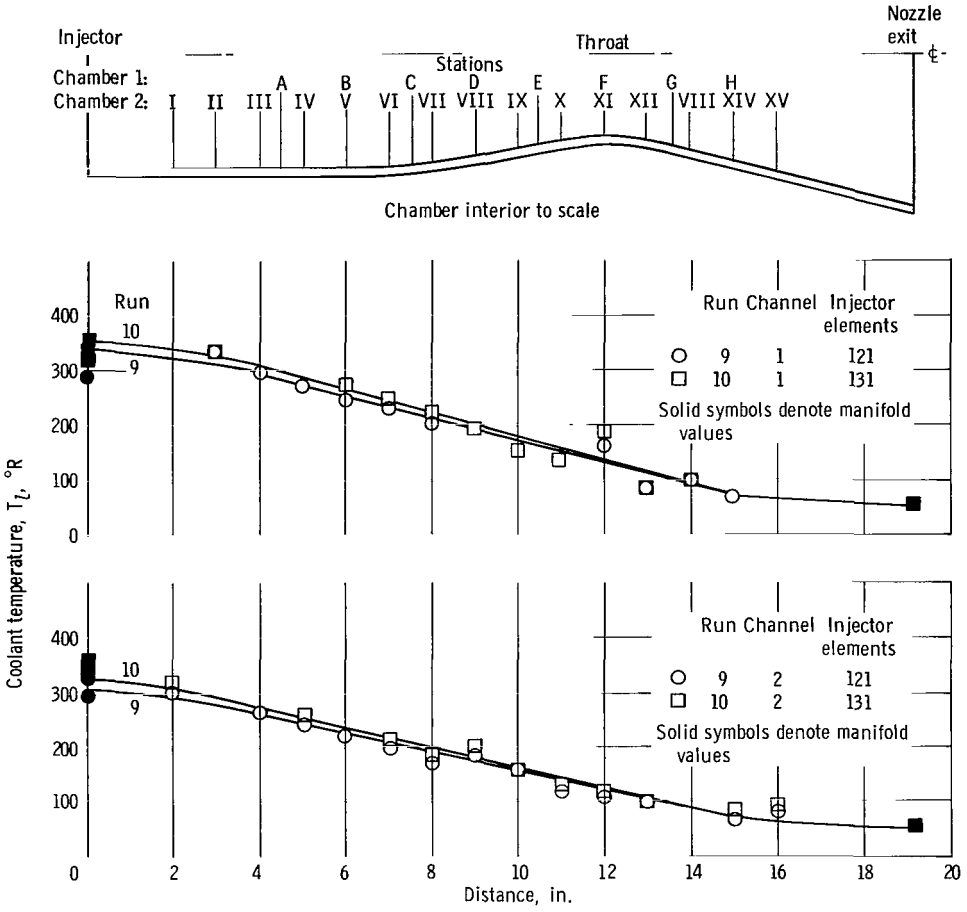

(c) 18 Percent hydrogen by weight.

Figure 7. - Concluded.

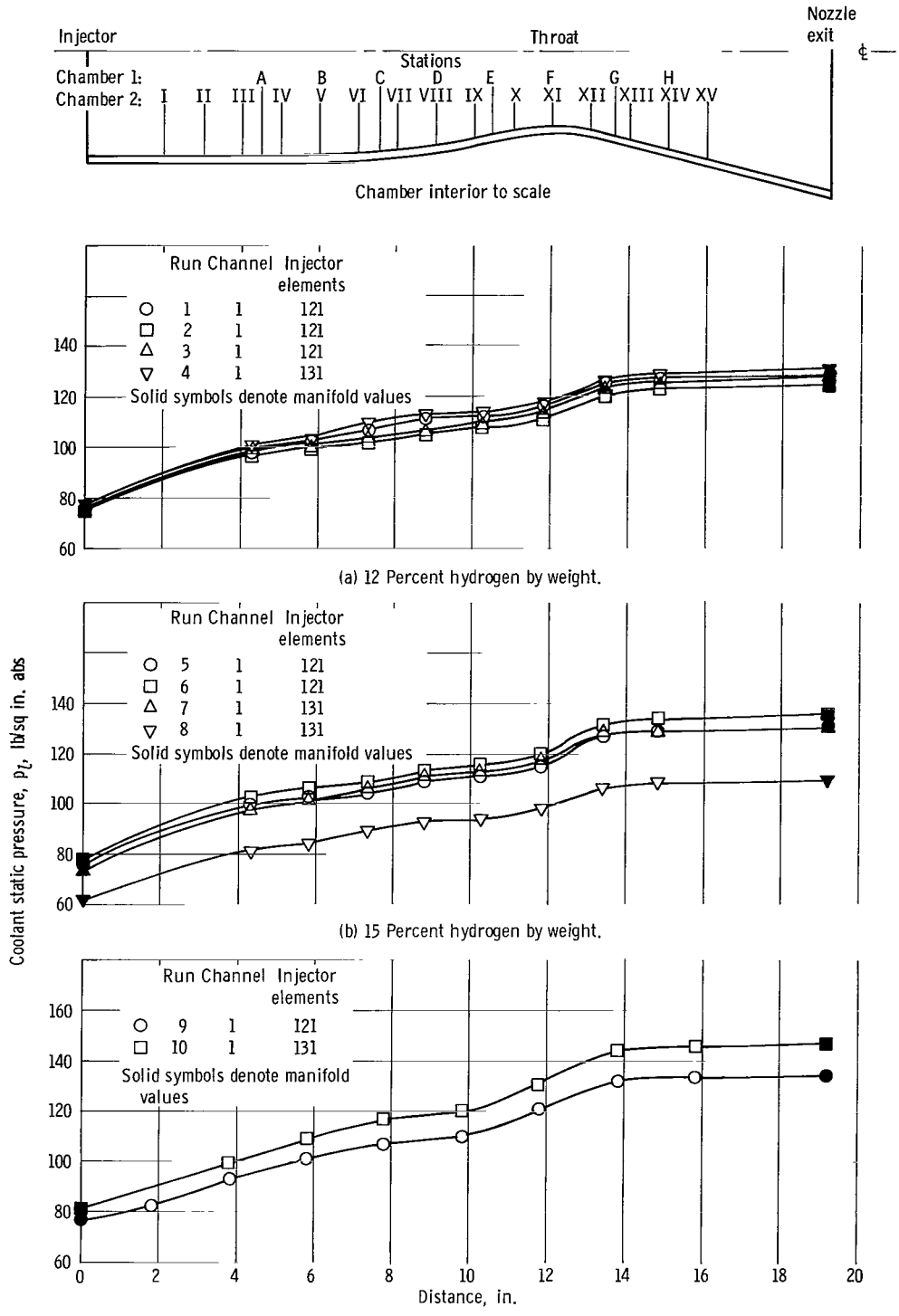

Figure 8. - Hydrogen-fluorine rocket engine thrust-chamber coolant static-pressure profiles obtained at 60-pounds-per-square-inch-absolute (50-lb/sq in. abs for run 8) combustion pressure.

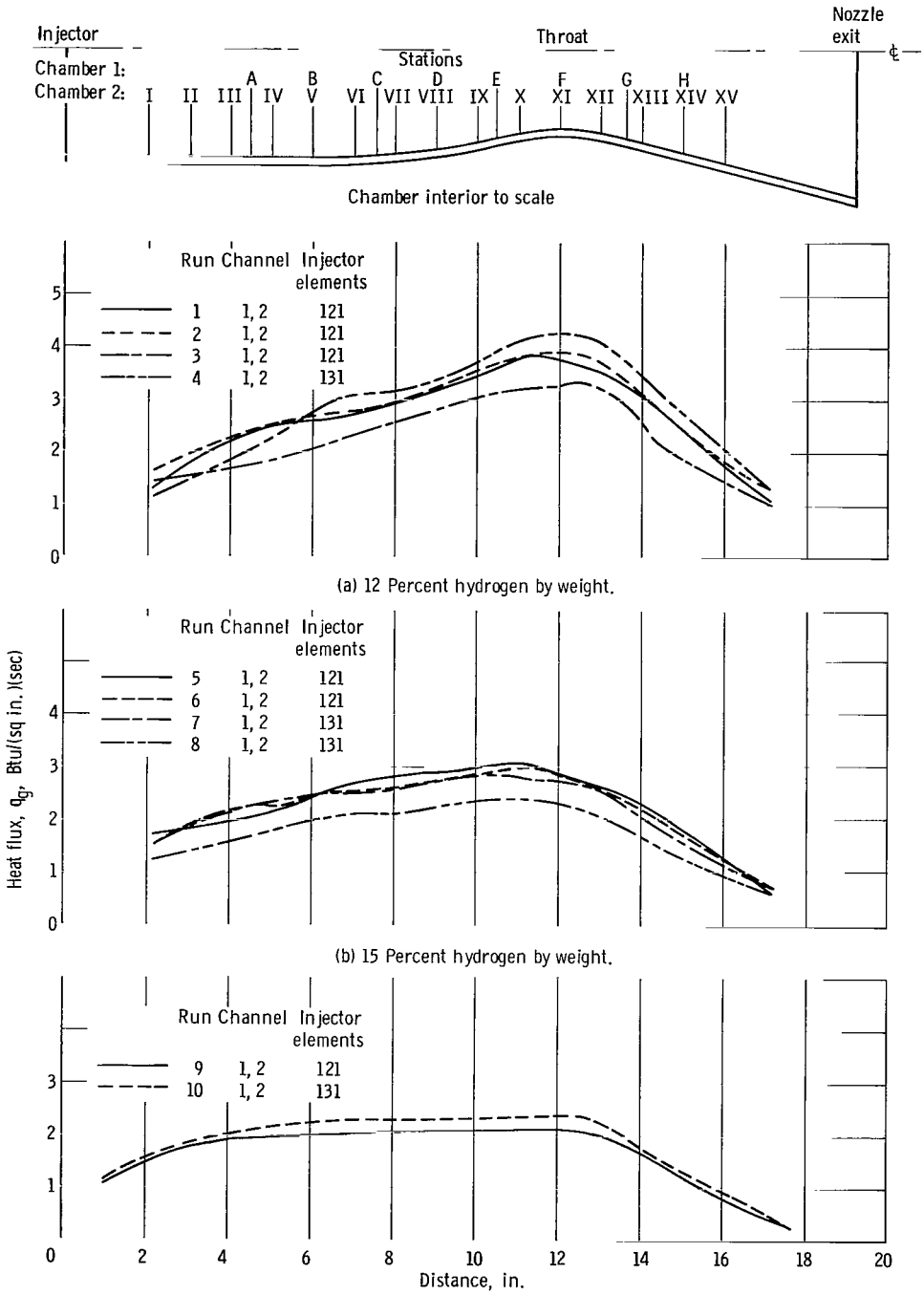

(a) 12 Percent hydrogen by weight.

(b) 15 Percent hydrogen by weight.

(c) 18 Percent hydrogen by weight.

Figure 9. - Thrust chamber axial heat-flux distributions for various propellant combination fuel weight fractions at 60-pounds-per-square-inch-absolute (50-lb/sq in. abs for run 8) combustion pressure.

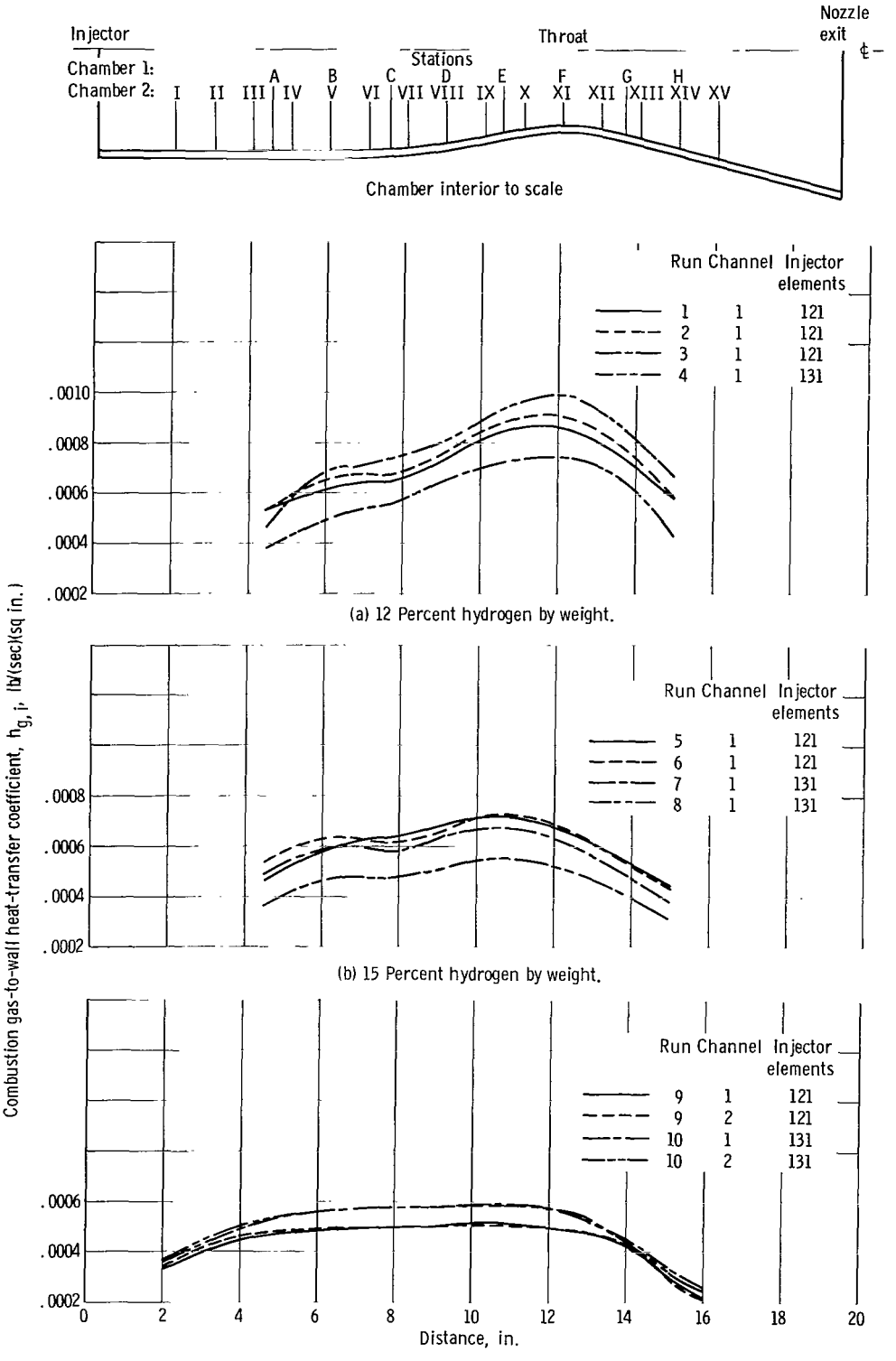

(a) 12 Percent hydrogen by weight.

(b) 15 Percent hydrogen by weight.

(c) 18 Percent hydrogen by weight.

Figure 10. - Combustion gas-to-wall heat-transfer coefficients for various propellant combination fuel weight fractions at 60-pounds-per-square-inch-absolute (50-lb/sq in. abs for run 8) combustion pressure.

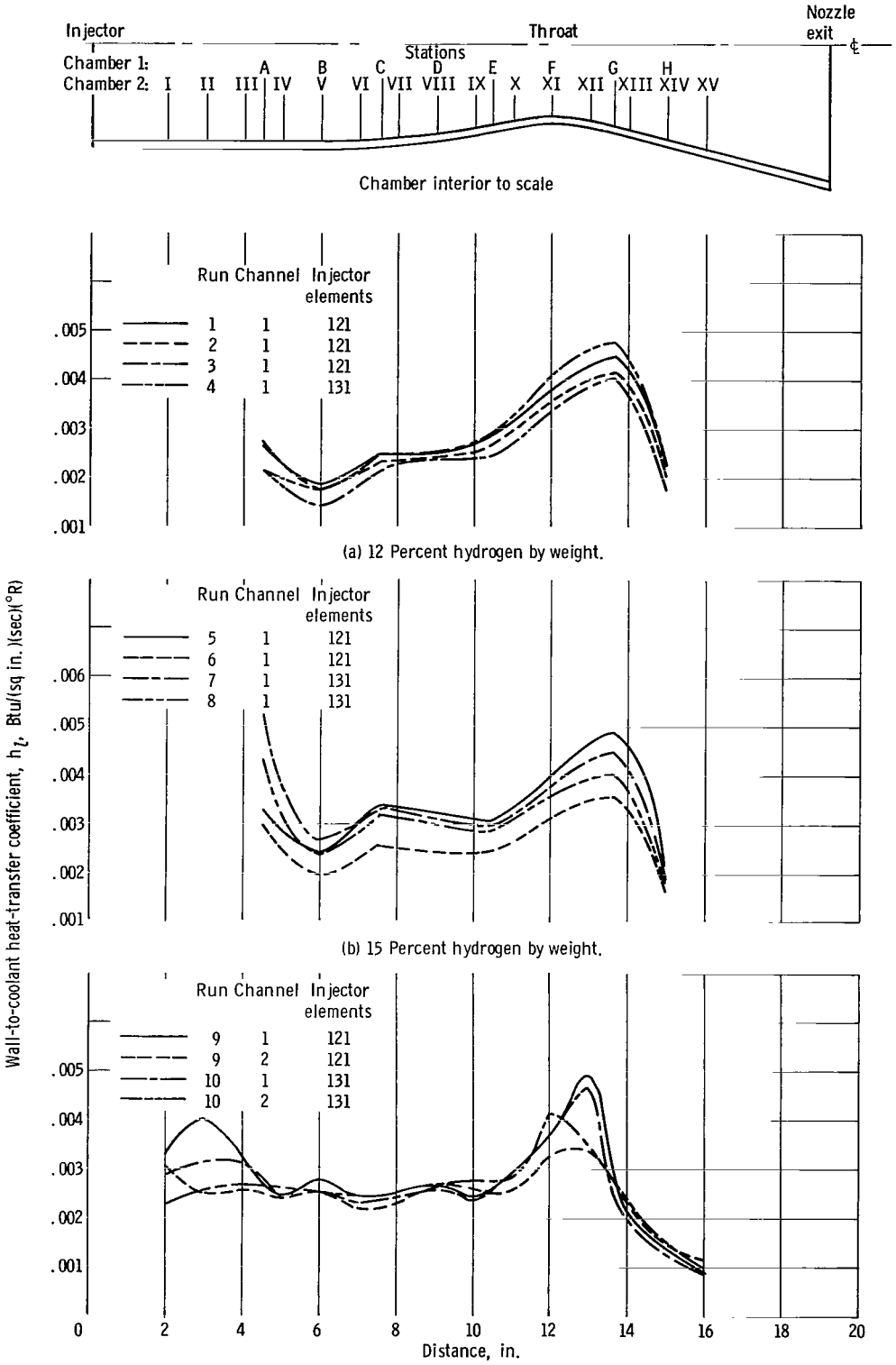

Figure 11. - Wall-to-coolant heat-transfer coefficients for various propellant combination fuel weight fractions at 60-pounds-per-square-inch-absolute (50-lb/sq in. abs for run 8) combustion pressure.

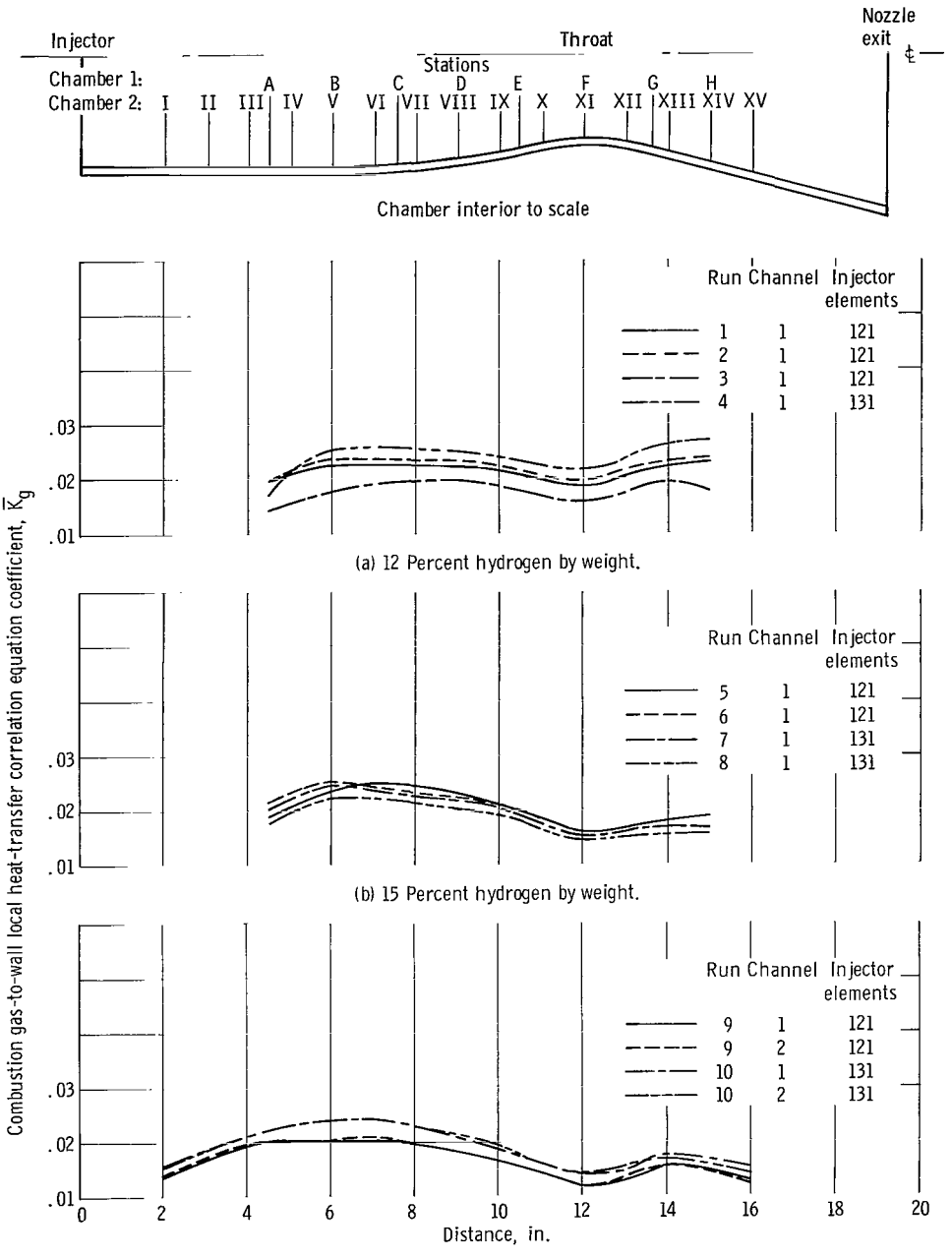

(a) 12 Percent hydrogen by weight.

(b) 15 Percent hydrogen by weight.

(c) 18 Percent hydrogen by weight.

Figure 12. - Combustion gas-to-wall local heat-transfer correlation equation coefficients for various propellant combination fuel weight fractions at 60-pound-per-square-inch-absolute (50-lb/sq in. abs for run 8) combustion pressure.

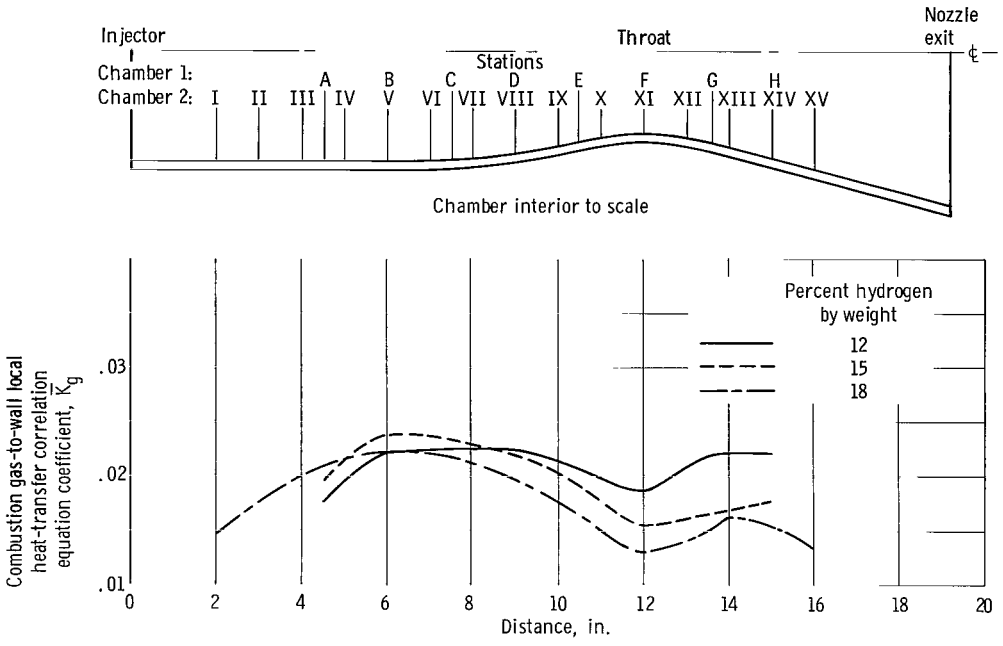

(d) Summary.

Figure 12. - Concluded.

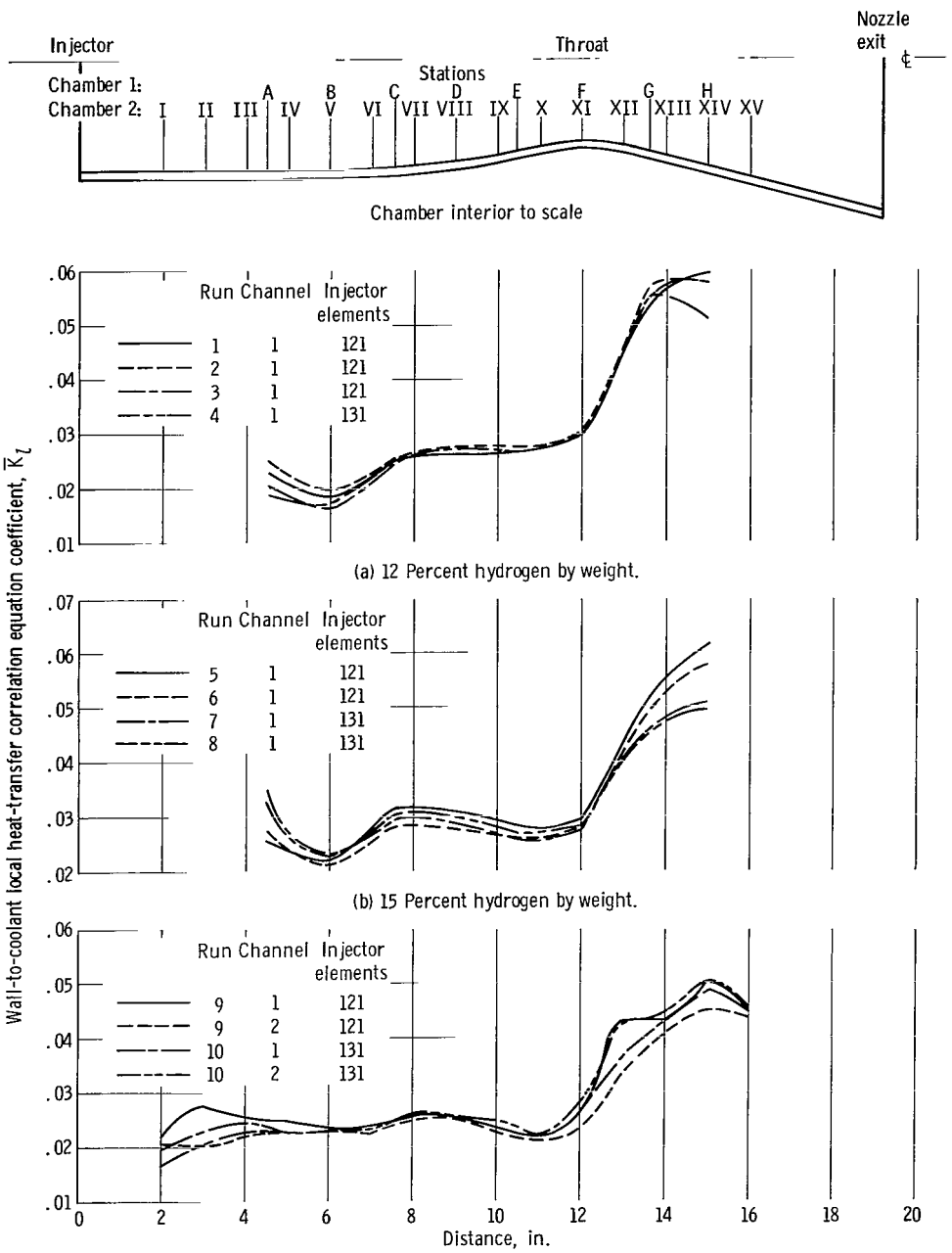

Figure 13. - Wall-to-coolant local heat-transfer correlation equation coefficients for various propellant combination fuel weight fractions at 60-pounds-per-square-inch-absolute (50-lb/sq in. abs for run 8) combustion pressure.

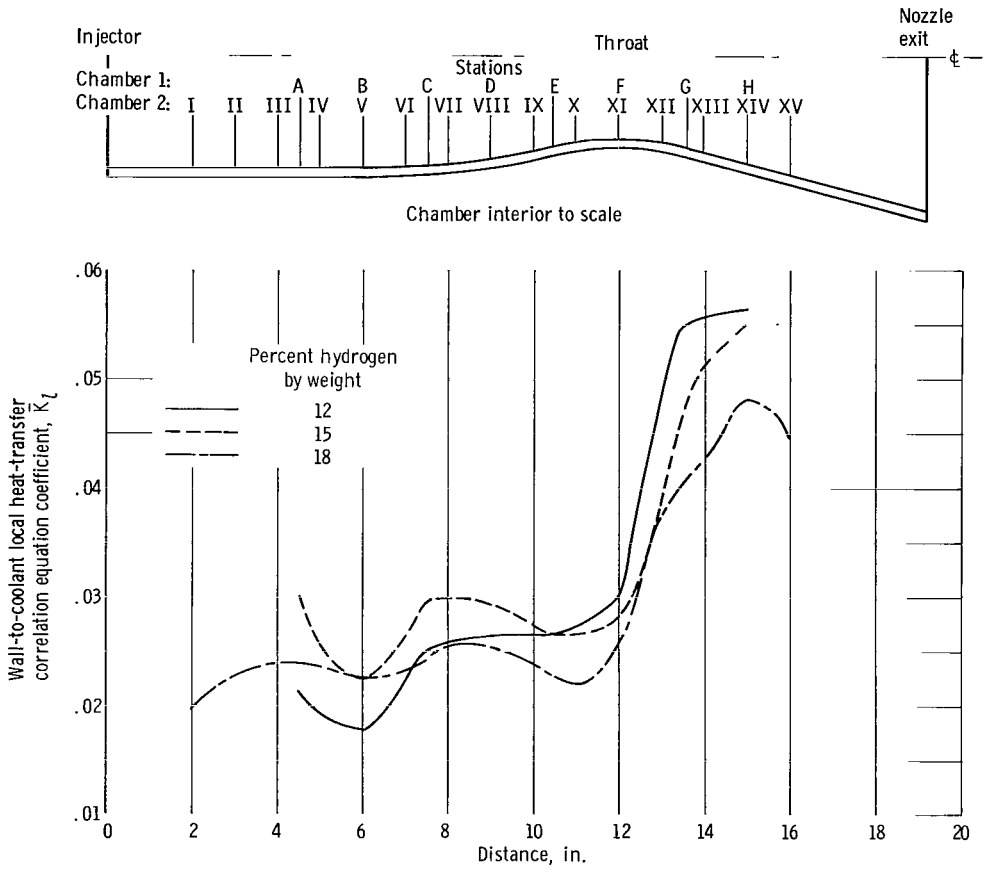

(d) Summary.

Figure 13. - Concluded.

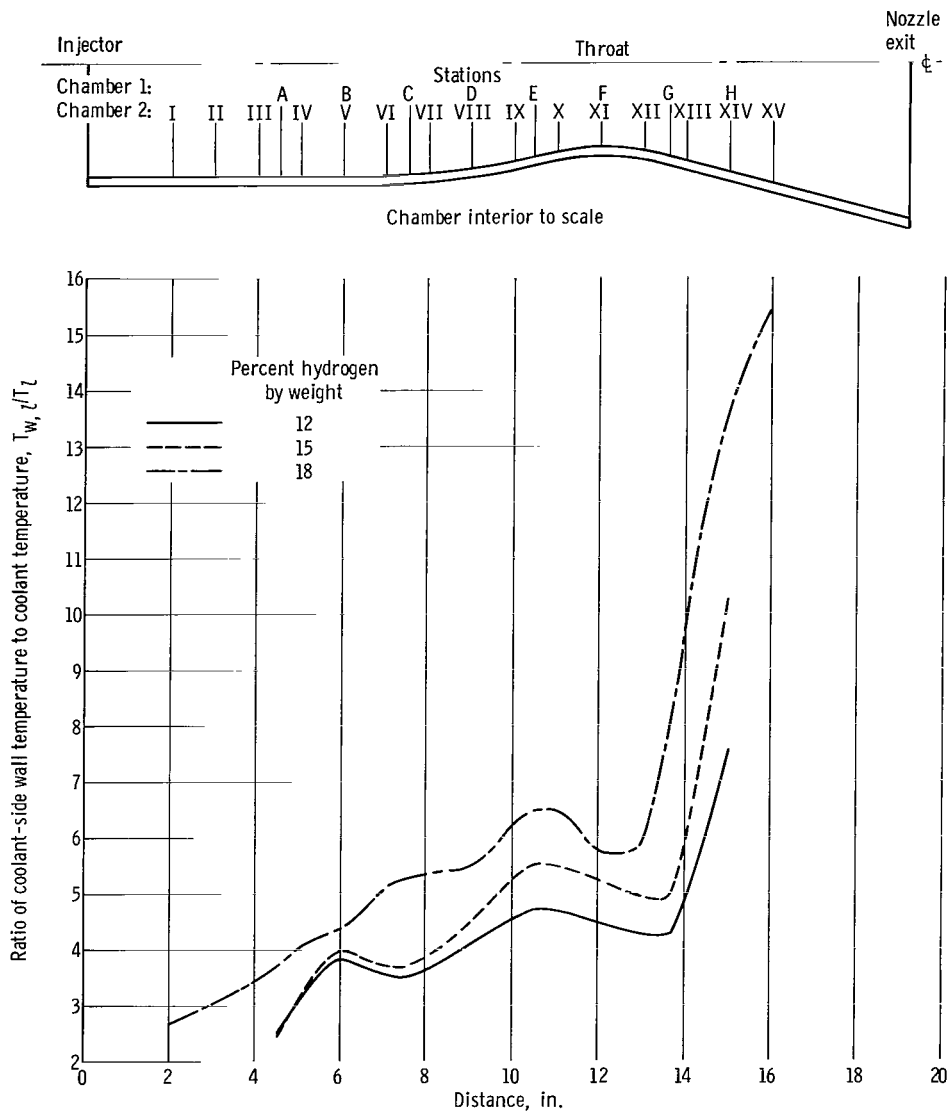

Figure 14. - Averaged values of ratio of coolant-side wall temperature to coolant temperature for various propellant combination fuel weight fractions.

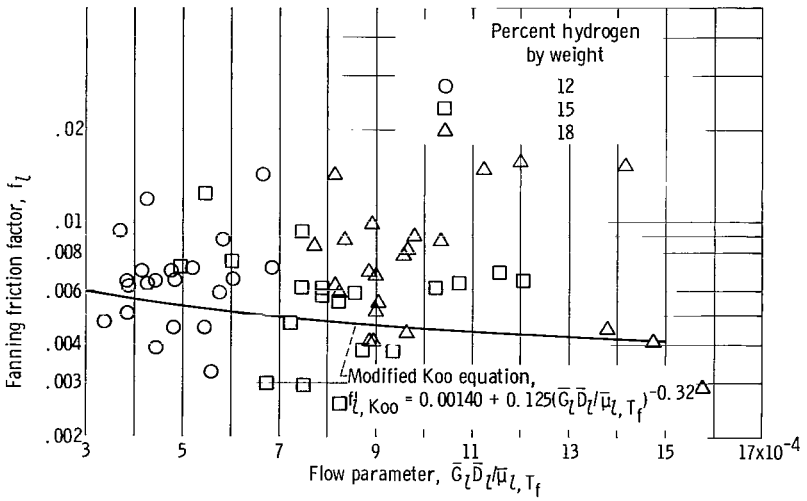

Figure 15. - Experimental coolant friction factors for various propellant combination fuel weight fractions.

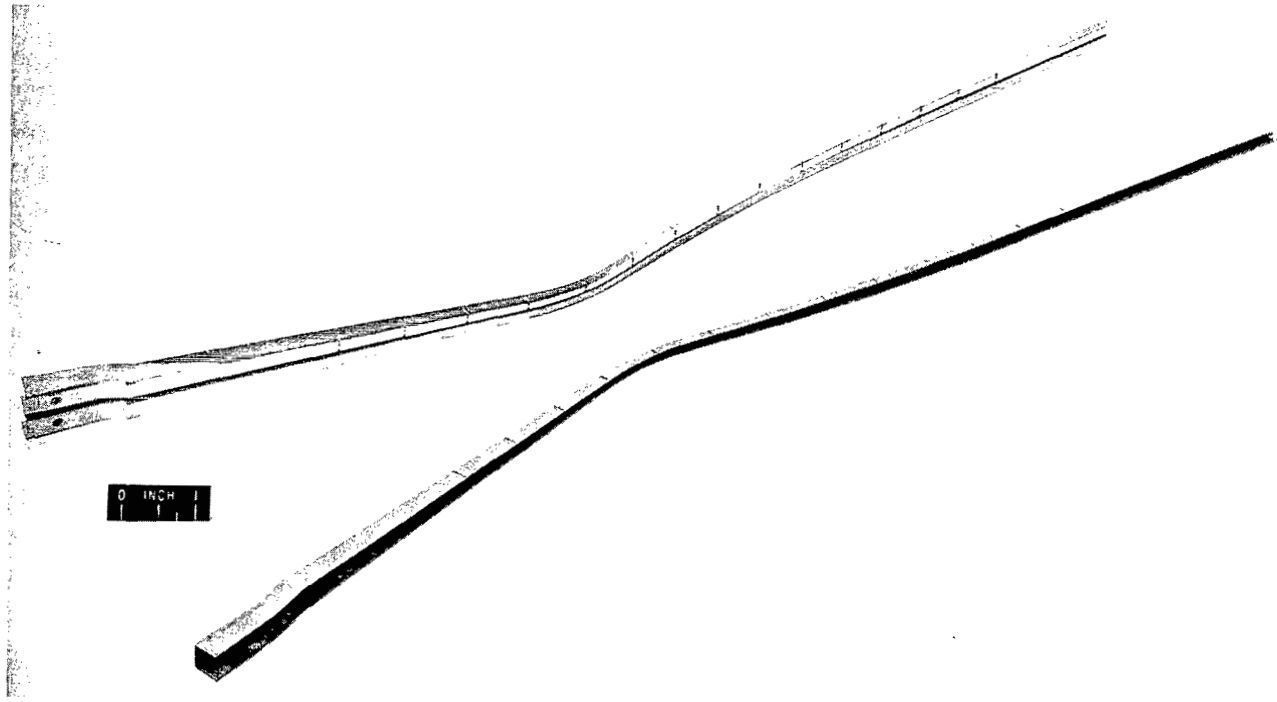

C-62530

(a) Channel group showing radial and transverse thermocouple slots located at 15 axial stations.

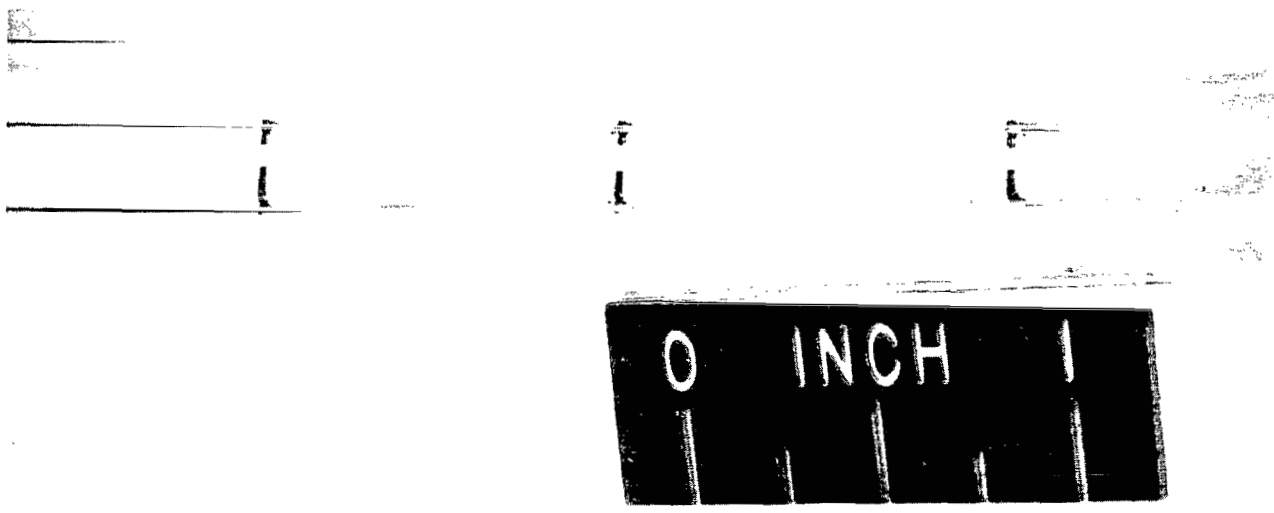

C-62531

(b) Detail of thermocouple slots in channel bottom.

Figure 16. - Thrust chamber 2 coolant channels preslotted for thermocouple placement.

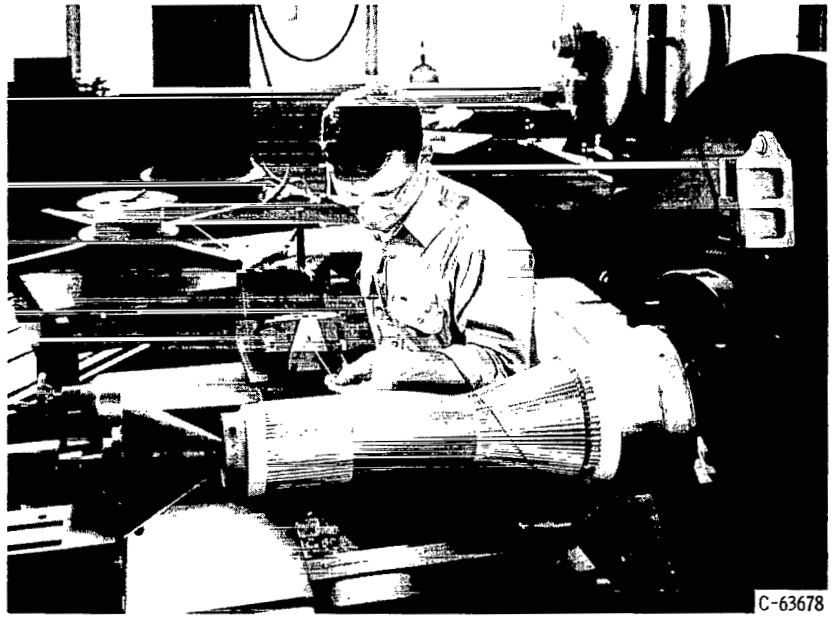

Figure 17. - Final wire-wrapping operation for thrust chamber 2.

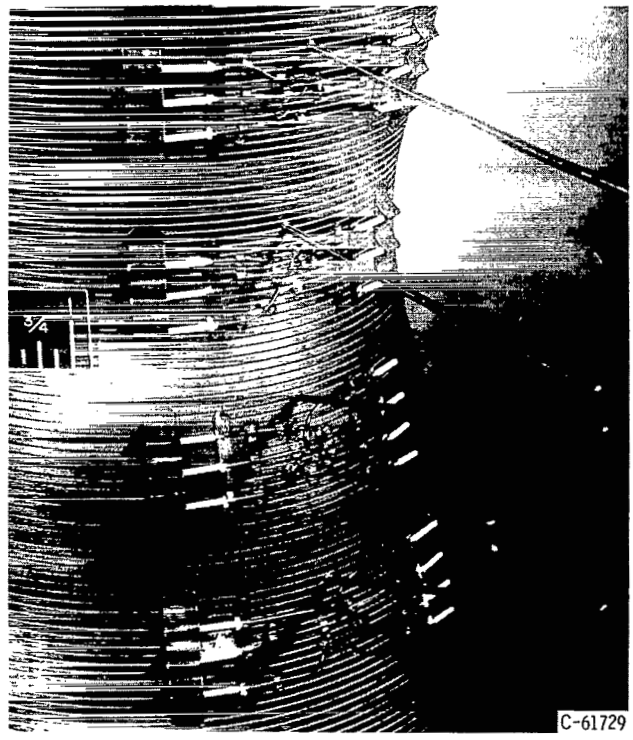

Figure 18. - Detail of external appearance of some instrument stations on thrust chamber 1 prior to final brazing operation.

Figure 19. - Thrust chamber 1 installed on test stand, showing protective cover and instrument connection systems. Ejector tube has been retracted here for clarity.

"The aeronautical and space activities of the United States shall be conducted so as to contribute . . . to the expansion of human knowledge of phenomena in the atmosphere and space. The Administration shall provide for the widest practicable and appropriate dissemination of information concerning its activities and the results thereof."

—NATIONAL AERONAUTICS AND SPACE ACT OF 1958

NASA SCIENTIFIC AND TECHNICAL PUBLICATIONS

TECHNICAL REPORTS: Scientific and technical information considered important, complete, and a lasting contribution to existing knowledge.

TECHNICAL NOTES: Information less broad in scope but nevertheless of importance as a contribution to existing knowledge.

TECHNICAL MEMORANDUMS: Information receiving limited distribution because of preliminary data, security classification, or other reasons.

CONTRACTOR REPORTS: Scientific and technical information generated under a NASA contract or grant and considered an important contribution to existing knowledge.

TECHNICAL TRANSLATIONS: Information published in a foreign language considered to merit NASA distribution in English.

SPECIAL PUBLICATIONS: Information derived from or of value to NASA activities. Publications include conference proceedings, monographs, data compilations, handbooks, sourcebooks, and special bibliographies.

TECHNOLOGY UTILIZATION PUBLICATIONS: Information on technology used by NASA that may be of particular interest in commercial and other non-aerospace applications. Publications include Tech Briefs, Technology Utilization Reports and Notes, and Technology Surveys.

Details on the availability of these publications may be obtained from:

SCIENTIFIC AND TECHNICAL INFORMATION DIVISION

NATIONAL AERONAUTICS AND SPACE ADMINISTRATION

Washington, D.C. 20546